










RESEARCH ARTICLE

Impoundment increases methane emissions in *Phragmites*-invaded coastal wetlands

Rebecca Sanders-DeMott¹  | Meagan J. Eagle¹  | Kevin D. Kroeger¹  |
 Faming Wang^{2,3}  | Thomas W. Brooks¹  | Jennifer A. O'Keefe Suttles¹  |
 Sydney K. Nick¹  | Adrian G. Mann¹  | Jianwu Tang² 

¹U. S. Geological Survey, Woods Hole Coastal and Marine Science Center, Woods Hole, Massachusetts, USA

²Marine Biological Laboratory, Woods Hole, Massachusetts, USA

³Xiaoliang Research Station for Tropical Coastal Ecosystems, Key Laboratory of Vegetation Restoration and Management of Degraded Ecosystems, and the CAS Engineering Laboratory for Ecological Restoration of Island and Coastal Ecosystems, South China Botanical Garden, Chinese Academy of Sciences, Guangzhou, China

Correspondence

Rebecca Sanders-DeMott, U. S. Geological Survey, Woods Hole Coastal and Marine Science Center, Woods Hole, MA 02543, USA.

Email: rsanders-demott@usgs.gov

Funding information

National Oceanic and Atmospheric Administration, Grant/Award Number: NA14NOS4190145; U.S. Geological Survey Coastal & Marine Hazards and Resources Program; U.S. Geological Survey - National Park Service Natural Resources Preservation Program, Grant/Award Number: 2021-07; U.S. Geological Survey Mendenhall Research Fellowship Program; U.S. Geological Survey LandCarbon Program

Abstract

Saline tidal wetlands are important sites of carbon sequestration and produce negligible methane (CH₄) emissions due to regular inundation with sulfate-rich seawater. Yet, widespread management of coastal hydrology has restricted tidal exchange in vast areas of coastal wetlands. These ecosystems often undergo impoundment and freshening, which in turn cause vegetation shifts like invasion by *Phragmites*, that affect ecosystem carbon balance. Understanding controls and scaling of carbon exchange in these understudied ecosystems is critical for informing climate consequences of blue carbon restoration and/or management interventions. Here, we (1) examine how carbon fluxes vary across a salinity gradient (4–25 psu) in impounded and natural, tidally unrestricted *Phragmites* wetlands using static chambers and (2) probe drivers of carbon fluxes within an impounded coastal wetland using eddy covariance at the Herring River in Wellfleet, MA, United States. Freshening across the salinity gradient led to a 50-fold increase in CH₄ emissions, but effects on carbon dioxide (CO₂) were less pronounced with uptake generally enhanced in the fresher, impounded sites. The impounded wetland experienced little variation in water-table depth or salinity during the growing season and was a strong CO₂ sink of $-352 \text{ g CO}_2\text{-C m}^{-2} \text{ year}^{-1}$ offset by CH₄ emission of $11.4 \text{ g CH}_4\text{-C m}^{-2} \text{ year}^{-1}$. Growing season CH₄ flux was driven primarily by temperature. Methane flux exhibited a diurnal cycle with a night-time minimum that was not reflected in opaque chamber measurements. Therefore, we suggest accounting for the diurnal cycle of CH₄ in *Phragmites*, for example by applying a scaling factor developed here of ~ 0.6 to mid-day chamber measurements. Taken together, these results suggest that although freshened, impounded wetlands can be strong carbon sinks, enhanced CH₄ emission with freshening reduces net radiative balance. Restoration of tidal flow to impounded ecosystems could limit CH₄ production and enhance their climate regulating benefits.

KEYWORDS

blue carbon, coastal wetland, dike, eddy covariance, impoundment, methane, net ecosystem exchange, *phragmites*, restoration, static chambers

This is an open access article under the terms of the [Creative Commons Attribution-NonCommercial](https://creativecommons.org/licenses/by-nc/4.0/) License, which permits use, distribution and reproduction in any medium, provided the original work is properly cited and is not used for commercial purposes.

© 2022 The Authors. *Global Change Biology* published by John Wiley & Sons Ltd. This article has been contributed to by U.S. Government employees and their work is in the public domain in the USA.

1 | INTRODUCTION

Coastal wetlands are a powerful sink for carbon (C) from the atmosphere due to their rapid rates of C uptake and slow rates of decomposition (Chmura et al., 2003; McLeod et al., 2011). In addition, the presence of sulfate-rich seawater in tidally influenced coastal ecosystems suppresses the production of methane (CH_4 ; Bartlett et al., 1987; DeLaune et al., 1983; Luo et al., 2019; Weston et al., 2006), a potent greenhouse gas (GHG). Therefore, with rapid C sequestration and minimal CH_4 production, the “blue carbon” stored in coastal wetlands is of high value for mitigating GHG emissions and is increasingly being looked to by various entities as a natural climate solution for C removal (McLeod et al., 2011; NASEM, 2019). Conserving healthy coastal wetlands to maintain their net climate regulating benefit is a priority within this natural climate solution framework, but there is also substantial promise for reining in CH_4 emissions and improving GHG balance by restoring coastal wetlands that have been degraded through extensive hydrological management (Kroeger et al., 2017). While the most effective strategy for avoiding the worst effects of climate change remains rapidly reducing fossil fuel carbon dioxide (CO_2) emissions, enhancing the climate regulating benefits of natural ecosystems is part of a comprehensive approach to tackle this grand challenge (IPCC, 2021).

Approximately one million ha of wetlands along the US coast are in a state of hydrological management, having been tidally restricted by barriers like dikes and transportation infrastructure (Crooks et al., 2018; Fargione et al., 2018; Kroeger et al., 2017). About half of these managed coastal wetlands are drained for alternative land uses, whereas the rest are impounded, meaning that the water is retained but tidal exchange is limited or excluded. While the global extent of coastal areas under this type of hydrological management is unknown, the high density of roadways fragmenting coastal landscapes worldwide (Ibisch et al., 2016) suggests that tidal restrictions are an important factor in the global decline of coastal wetlands over the last century (Li et al., 2018) and are widespread (Kroeger et al., 2017). Impoundment leads to a suite of changes that affect wetland function, including shifts in salinity, water level dynamics, frequency and extent of tidal flushing, and vegetation communities (Portnoy, 1999; Roman et al., 1984). These changes, particularly freshening and reduced sulfate supply that can drive CH_4 production (Bartlett et al., 1987; Poffenbarger et al., 2011; Wang et al., 2017; Windham-Myers et al., 2018), are likely to alter the GHG balance of the ecosystem and increase net radiative forcing (Kroeger et al., 2017). Although there is a high degree of uncertainty regarding the total area (Holmquist et al., 2018) and restoration potential (Crooks et al., 2018) of tidally restricted coastal wetlands, recent estimates suggest that up $12 \text{ Tg CO}_2\text{-eq year}^{-1}$ of CH_4 emission could be avoided if impounded ecosystems in the United States alone were restored to a state of natural tidal exchange (Fargione et al., 2018).

Reducing CH_4 emission, which has a sustained global warming potential 45 times that of CO_2 over a century (Neubauer & Megonigal, 2015), is a critical component of the effort to rapidly scale back atmospheric GHG concentrations (IPCC, 2021) and

an emerging priority focus of global climate policy (e.g., Global Methane Pledge of November 2021). As infrastructure ages and sea levels rise, management decisions for coastal areas are increasingly pressing. Although there are many competing priorities influencing coastal decision-making, a better understanding of the GHG consequences of management options should be of increasing importance for coastal stakeholders. In fact, tidal wetland restoration projects are now eligible to generate carbon credits in voluntary and certain compliance markets via global and national standards (Clean Energy Regulator, 2022; Needleman et al., 2018). But, although blue carbon ecosystems are already being incorporated into national emissions reductions targets (Herr & Landis, 2016), guidelines for national GHG inventories do not account for the potential of avoided CH_4 emissions (IPCC, 2014). Thus, it is critical to gain a better, scalable understanding of how CH_4 emission change with restoration scenarios to advance this climate mitigation opportunity.

Empirical data on impounded coastal ecosystems, which have distinct characteristics from their natural counterparts, are scarce and relatively few continuous data sets on gas exchange like those derived from eddy covariance exist for coastal ecosystems (Knox et al., 2019; Lu et al., 2017). In impounded ecosystems, freshening often occurs due to reduced seawater exchange and retained ground or surface water from fresh, upland sources (Burdick et al., 2001). In the eastern United States, freshening due to tidal restrictions and impoundments is particularly associated with increased competitive advantage and subsequent invasion by non-native *Phragmites australis* (hereafter *Phragmites*) (Roman et al., 1984). The net effect of the rapid growing, deep-rooted *Phragmites* on ecosystem CO_2 and CH_4 balance remains unresolved due to counteracting influences of *Phragmites* on wetland biogeochemistry (Armstrong et al., 2006; Emery & Fulweiler, 2014; Martin & Moseman-Valtierra, 2015; Windham, 2001). As a result of these complex interactions, the effects of changes to salinity with invasion by *Phragmites* may manifest in unique ways compared to other wetland vegetation.

A better understanding of how salinity and impoundment affect CH_4 and CO_2 fluxes in coastal wetlands dominated by *Phragmites* is needed to improve predictions of how tidal restoration would change CH_4 emissions and ultimately radiative balance. The objectives of this study were to (1) investigate whether the widely observed influence of salinity on CH_4 emissions is maintained across impounded versus tidally unrestricted ecosystems dominated by *Phragmites* and (2) to probe the specific drivers of CH_4 and CO_2 fluxes within a *Phragmites*-invaded impounded wetland. We used both static chambers to assess C fluxes across a salinity gradient along with eddy covariance to more thoroughly explore the patterns and magnitude of annual C exchange in an impounded wetland. We hypothesized that reduced salinity in impounded sites would result in greater CH_4 emissions and that low variability in salinity and water-table depth in impounded ecosystems, due to limited tidal activity and hydrologic flushing, increases the importance of other factors, like temperature, in controlling CH_4 and CO_2 exchange. In addition, by employing two complementary tools for assessing C fluxes (static chambers and eddy covariance), we gained insight into approaches for scaling

measured fluxes in coastal wetlands to management-relevant metrics to support assessment and monitoring of C exchange for blue carbon applications.

2 | METHODS

2.1 | Site descriptions

The Herring River (41.9380, -70.0552) is a 400-ha diked estuary complex that is part of the Cape Cod National Seashore in Wellfleet and Truro, MA, with mean annual temperature of 10.3°C and 1153 mm of annual precipitation from 1991 to 2020 (Arguez et al., 2012) (Figure 1). Dike construction across the main channel in 1908, along with continued management of upstream waterways, has created an estuary complex composed of both impounded and drained areas where freshwater vegetation such as *Phragmites*, *Typha*, various shrub species, and woodland have replaced former salt marsh habitat (Portnoy, 1999). This study examines sites within a monodominant *Phragmites* stand in a mesohaline impounded zone located approximately 1 km landward of the dike and adjacent to the main channel (Figure 1e). Two sites were established between the main channel and the upland forest edge. Despite their proximity, the sites have consistent differences in salinity, with the low salinity site closer to the main channel (hereafter *Impounded-Low*) and the high salinity site closer to the forest edge (hereafter *Impounded-High*). Both sites are within 65 m of an eddy covariance tower (Ameriflux Site Code US-HRP, described below) and are representative of the dominant land cover within the tower footprint (Figure S1).

Sage Lot Pond marsh (41.5583, -70.5039) is a 119-ha natural salt marsh complex with natural, unrestricted tidal exchange located within the Waquoit Bay National Estuarine Research Reserve in Falmouth, MA on Cape Cod with mean annual temperature of 10.7°C and 1219 mm of annual precipitation from 1991 to 2020 (Arguez et al., 2012; Figure 1). Vegetation in the low marsh is dominated by *Spartina alterniflora*, while the high marsh community is composed of *Spartina patens*, *Distichlis spicata*, *Juncus gerardii*, and various *Salicornia* species with *Phragmites* encroaching from the forested upland edges (Wang et al., 2016). We established two sites along an axis from the bay toward the inland marsh edge. The site closer to the bay experiences more frequent tidal inundation and more saline waters (hereafter *Unrestricted-High*) than the inland site, which is at a higher elevation and where fresh groundwater contributes to lower salinity (hereafter *Unrestricted-Low*; Figure 1f).

2.2 | Environmental measurements and vegetation characteristics

In June 2020, we constructed boardwalks at all sites to allow for repeated sampling with minimal disturbance. At each site we installed a ~30 cm deep 3-cm-diameter PVC well screened from 0 to 20 cm depth and equipped to monitor water-table depth relative

to the soil surface, salinity, and water temperature (In-Situ Inc.; Aqua TROLL 200). Due to abnormally dry conditions across Cape Cod that began in July and persisted through December 2020 (USDM, 2021), water table at the *Unrestricted-Low* site dropped below the 20-cm depth deployment of the original water-level sensor. All well data presented after July 2020 for the *Unrestricted-Low* site is from a deeper well (80 cm, screened 10–70 cm depth; 65 cm deep sensor) that was added to account for the shallow water-table depth. Wells were coupled with temperature sensors in the canopy at 1 m height and soil temperature at 10-cm depth (HOBO Pro v2; Onset HOBO Pro v2). At one location at Herring River (eddy covariance tower) and one location at Sage Lot Pond (*Unrestricted-High*), we measured above canopy air temperature and relative humidity (Onset HOBO Temperature/RH Smart Sensor S-THB-M00x), barometric pressure (In-Situ Inc.; Rugged BaroTROLL), and incoming photosynthetically active radiation (PAR; Onset HOBO Photosynthetically Active Radiation Smart Sensor S-LIA-M003).

To characterize differences in vegetation density across sites, we conducted a survey of live *Phragmites* culm density, along with mean height and diameter in early September 2020 prior to senescence. We non-destructively measured five evenly spaced 1-m² quadrats around both a 4- and 8-m radius circle centered on the chambers ($n = 10$ per site). We then estimated biomass using both height and diameter according to a *Phragmites*-specific allometric equation (Lu et al., 2016).

2.3 | Static chamber flux measurements

Static chamber CH₄ and CO₂ flux measurements were collected five times per site from the mid- to late-growing season in 2020 on July 21, August 19, September 15, October 14, and November 9 at the unrestricted sites at Sage Lot Pond and on July 28–29, August 25–26, September 23, October 19, and November 18 at the impounded sites at Herring River. Round 3/16" thick PVC collars (55-cm inner diameter, 24-cm height) were inserted into the sediment surrounding intact vegetation to a depth of at least 10 cm more than 4 weeks prior to sampling. The collars were sharpened on the bottom edge and a serrated knife and reciprocating saw were used to cut through roots to reduce compaction of the sediment. There were two 1.3-cm holes drilled 3 cm from the collar bottom to allow equilibration of water below the surface and another 1.6-cm hole at the sediment surface to allow for drainage of surface water, which was plugged with a rubber stopper during sampling. The three collars per site were all within 2 m of the well and temperature sensors.

We used a modular system of 3/8" thick clear, round acrylic chambers (California Quality Plastics, Inc.) to enclose the vegetation and sediment surface for flux measurement (Figure S2). Chamber sections were 55-cm diameter and 0.91 m tall. Depending on the height of the vegetation at the sampling location, we used either two (unrestricted sites at Sage Lot Pond) or three (impounded sites at Herring River) stacked chambers for a total chamber height of 1.83 or 2.74 m and empty chamber volume of 0.43 or 0.64 m³, respectively. The

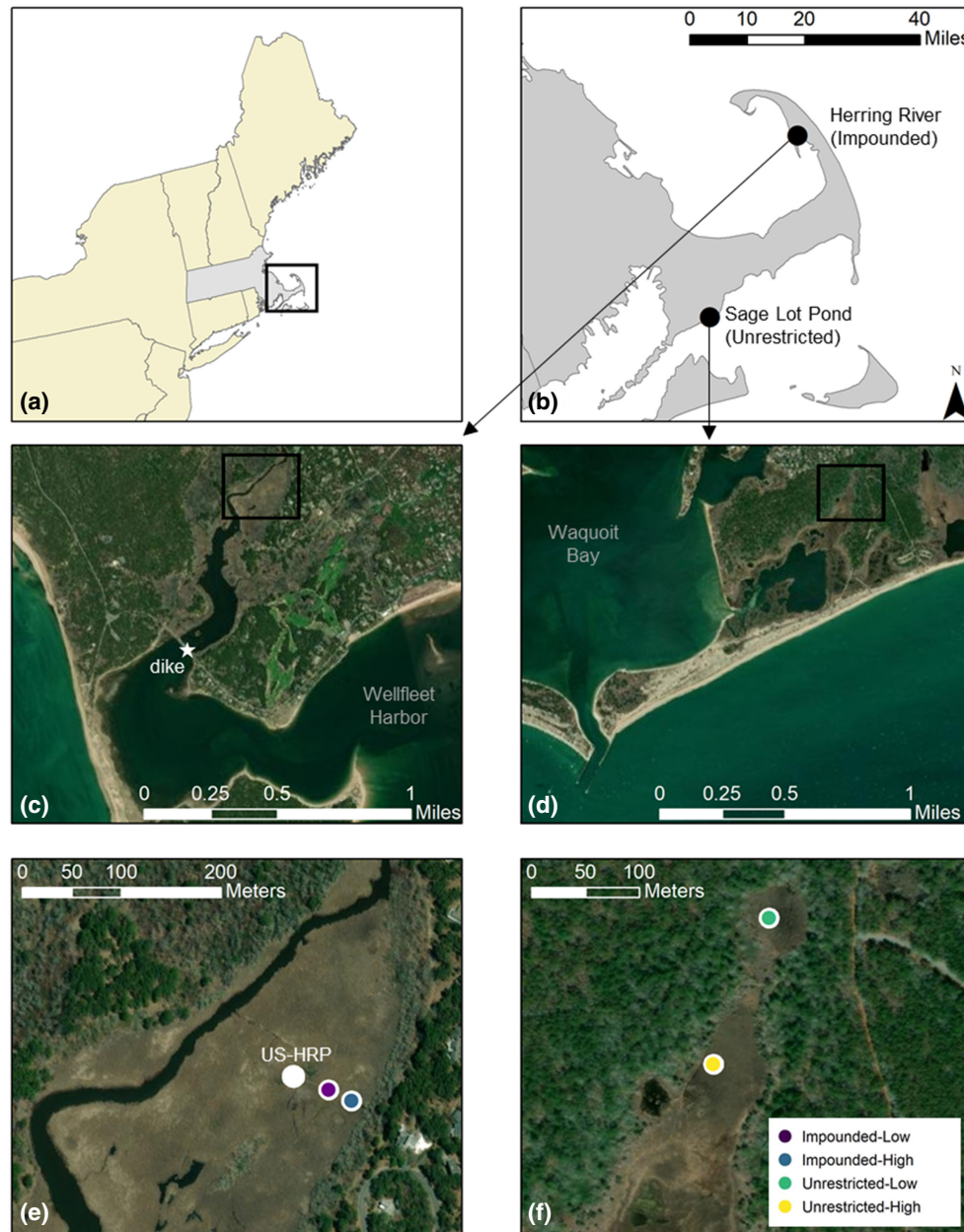


FIGURE 1 Map illustrating the location of sites relative to the (a) northeastern United States and (b) Cape Cod. (c) the dike-impounded Herring River is hydrologically restricted from tidal exchange with Wellfleet Harbor while the (d) unrestricted estuary at sage lot pond is open to tidal activity from Waquoit Bay. The black rectangles in panels (c) and (d) indicate the locations of panels (e) and (f), respectively. (e) the location of the eddy covariance tower at Herring River (Ameriflux site code US-HRP) is shown, along with the *impounded-low* and *impounded-high* sites between the main channel and forest edge (f) the *unrestricted-high* and *unrestricted-low* sites at sage lot pond are distributed along an axis from the bay towards the upland forest. Map image is the intellectual property of Esri and is used herein under license. Copyright © 2014 Esri and its licensors. All rights reserved. [Colour figure can be viewed at wileyonlinelibrary.com]

topmost chamber always had a transparent lid permanently affixed with silicone caulking and a vent tube to allow for pressure equilibration. Once the chambers were stacked, the junction between sections was sealed with a 5 cm wide self-amalgamating gas and water-impermeable silicone tape (Rescue Tape; Seal It Services, Inc.). Two battery-powered fans (10 cm in diameter) were attached to the inside of the chamber to homogenize air, and temperature sensors (HOBO Tidbit v2; Onset HOBO Tidbit v2) were mounted

to the inside of the top and bottom chambers to record chamber air temperature. On each sampling date, we counted the number, mean height, and diameter of living and standing dead *Phragmites* culms within each collar. We also recorded the actual height of the collar wall above the soil or water surface and the mean depth of the litter layer to accurately assess total volume. Soil volumetric water content integrated over the top 5 cm was measured (Meter Group Inc., TEROS-10) just outside each collar after gas sampling. All samples

were collected during mid-day hours between 10:00 and 14:00 local standard time.

Changes in concentrations of CH₄ and CO₂ during the incubation were measured using a portable optical feedback-cavity enhanced absorption spectrometer (LI-7810 CH₄/CO₂/H₂O Trace Gas Analyzer; LI-COR, Inc.) sampling at 1 Hz. The gas analyzer was attached to the chamber with ¼" nylon tubing (of varying length from 220 to 457 cm depending on the number of chambers used) via a sampling port in the topmost chamber and recirculated into the chamber via a port at the base. Incubations were conducted for 3–7 min, based on visual inspection of the stability of a linear concentration change in the gases of interest. Chamber flux incubations were conducted both in the light to quantify net ecosystem exchange (NEE), and in the dark to quantify ecosystem respiration (RECO) in the absence of photosynthesis. Dark measurements were made after light measurements were completed by covering the outside of the chamber with an opaque bubble reflective foil insulation (US Energy Products). The top chamber section was removed between the transparent and opaque incubations to ventilate and avoid oversaturation of the chamber air with CH₄ only if chamber CH₄ concentrations were over 3500 ppb, a threshold below the range where CH₄ saturation has been observed in static chamber methodological studies (Juszczak, 2013).

We used a sliding regression ("rollRegres" package in R, Christoffersen, 2019) to identify the 150-s window during the incubation where a simple linear regression of CH₄ or CO₂ concentration by time had a maximum R^2 . Most measurements (98% of CH₄ measurements, 67% of CO₂ measurements) had an $R^2 > .90$ (CH₄ mean $R^2 = .99$, $sd = 0.02$, $n = 60$; CO₂ mean $R^2 = .87$, $sd = 0.19$, $n = 60$). However, samples collected with slopes near 0 had low R^2 values (Figure S3), reflecting the low fluxes from those chambers that result in a small dependence of gas concentration on time. We therefore retained measurements where R^2 was below 0.90 for a given gas (usually CO₂) if the slope for the other gas (e.g., CH₄) measured concurrently did have a high $R^2 (>.90)$, indicating no leakage or other experimental error (Moseman-Valtierra et al., 2016). We verified that all linear models used to calculate flux had a significant slope ($p < .001$) and an RMSE ≤ 1 ppm for CO₂ and ≤ 10 ppb for CH₄. One measurement did not have a slope significantly different than 0, and that flux was therefore set to 0. We also monitored each chamber incubation for rapid changes in CH₄ concentration over time that deviated from the typical steady linear accumulation of CH₄ as a signal of potential ebullition. When potential ebullition was observed, in addition to applying the sliding 150-s linear regression described above, we estimated flux based on the total accumulation of CH₄ over the length of the entire incubation as the difference between the initial and final concentration of measured CH₄ (Needelman et al., 2018). The rate of concentration change of CO₂ and CH₄ (linear slope or the total CH₄ accumulation over time when ebullition was suspected) was converted to an area-based flux as per Davidson et al. (1998) using the volume and footprint of the chamber, along with measured chamber air temperature (pooled across the two temperature sensors) and field measured air pressure. Calculations

were executed with the "conc_to_flux" function in the R package "ecoflux" (Shannon, 2018). Chamber volume was corrected based on the tubing volume and number, height, and diameter of live and dead *Phragmites* culms in each individual chamber (assuming perfect cylinders), as well as the actual measured depth of the chamber collar above the sediment or water surface and the depth of the litter layer, which was assumed to have a 50% pore space. However, the calculated flux error associated with accounting for vegetation volume in the chamber was on average less than -2.5% relative to the empty chamber. Gross primary production (GPP) for each chamber measurement was calculated using NEE from the transparent incubation and RECO from the opaque incubation as $GPP = RECO - NEE$ for comparison with data from the eddy covariance tower.

2.4 | Eddy covariance ecosystem flux measurements

An eddy covariance system was originally installed at the Herring River site in 2017 to collect ecosystem scale measurements of CO₂ and CH₄ fluxes across the land surface (Ameriflux code US-HRP). A tripod tower was equipped with a LI-7500A open path CO₂/H₂O analyzer (LI-COR, Inc.) and a LI-7700 open path CH₄ analyzer (LI-COR, Inc.), along with a CSAT-3 3-D sonic anemometer (Campbell Scientific). Instruments are deployed at 4.4 m height above the ground surface, along with the suite of meteorological sensors described above (§ 2.2) that measure air temperature and humidity, incoming photosynthetically active radiation, and barometric pressure, along with precipitation (Onset HOBO Rain Gauge Smart Sensor S-Rgx-M002). Continuous measurements of salinity, water temperature, water-table depth, and soil temperature were recorded at the two chamber flux sampling sites at Herring River (Figure 1e) that are representative of the tower footprint and mean values from the two sites were used for all eddy covariance analysis. Eddy covariance data were collected at a frequency of 10 Hz and ancillary meteorological data were collected every 5 min (or 15 min for well metrics and soil temperature). Here we present 1 year of data collected from late-May 2020 through late-May 2021, with an approximately 4-week gap in data collection from late-September to late-October and another 2.5-month gap in CH₄ data collection from December–February due to instrument malfunction.

Half-hourly fluxes of CO₂ and CH₄ were computed from the covariation of high-frequency vertical wind direction and CO₂ and CH₄ concentration (Baldocchi, 2003) using the EddyPro software package (version 7.0.6, LI-COR, Inc.). Raw high frequency data were despiked (Vickers & Mahrt, 1997) and a double coordinate rotation was applied to anemometer measurements (Wilczak et al., 2001) along with a flux correction for the effects of humidity on sonic air temperature (Van Dijk, & Dolman, 2004), high-frequency and low-frequency spectral attenuations (Moncrieff et al., 1997), and air density fluctuations (Webb et al., 1980) coupled to instrument-related sensible heat flux in the winter (Burba et al., 2008). Footprint modeling to verify the sampling area was

performed (Kljun et al., 2015). We report fluxes as NEE, where negative values indicate net uptake of gas by the land surface and positive values indicate net loss of gas to the atmosphere. We removed low quality measurements (>1 per Mauder & Foken, 2006 quality flag, where 0 = highest quality fluxes, 1 = fluxes suitable for annual budget analysis, 2 = fluxes that should be discarded due to low quality), measurements made during and immediately following precipitation events, and any measurement collected during site maintenance or known instrument malfunction. We also removed measurements made during low-turbulence conditions with potential advective losses (Aubinet, 2008) and when friction velocity, u^* , was below a site-specific threshold of 0.118 m s^{-1} (Papale et al., 2006). To account for uncertainty in u^* threshold estimation, bootstrapping (100 iterations) was applied to u^* threshold estimation, and we report a range of cumulative fluxes calculated based on the 5% (0.082 m s^{-1}) and 95% (0.163 m s^{-1}) estimates (Papale et al., 2006; Wutzler et al., 2018). Instrument malfunction caused a gap in some meteorological data from late-January through mid-April 2021, and missing data (relative humidity and PAR) were filled with data from a nearby monitoring station to enable gapfilling of gas fluxes (EPA, 2021). Overall, we retained 65% of annual half-hourly measurements (54% of nighttime fluxes and 69% of daytime fluxes) for CO_2 and 56% (44% of nighttime fluxes and 61% of daytime fluxes) for CH_4 . Gapfilling of half-hourly CO_2 fluxes was performed using the marginal distribution sampling methodology and NEE was partitioned into its component fluxes, GPP and RECO, based on nighttime fluxes as a proxy for daytime respiration (Reichstein et al., 2005). We selected the nighttime partitioning approach because nighttime turbulence is relatively high and diurnal temperature variation is relatively modest at this coastal site providing a reasonable overlap of day and night conditions. In addition, due to the impounded state of the wetland, tidal cycles were not an important consideration for nighttime partitioning (see Results). All u^* estimation, CO_2 flux gapfilling, and partitioning were conducted with the R-based eddy covariance processing tool, "REddyProc" (Wutzler et al., 2018). Gapfilling of half-hourly CH_4 fluxes was performed using a random forest model, which included air temperature, soil temperature, water temperature, relative humidity, PAR, water-table depth, salinity, NEE, vapor pressure deficit, latent heat exchange, and air pressure (Kim, Johnson, et al., 2020).

2.5 | Data and statistical analysis

All carbon flux and environmental data reported here are available in Sanders-DeMott et al. (2022) and O'Keefe Suttles, Eagle, Sanders-DeMott, et al. (2022). Data and statistical analyses were conducted in R v. 4.0.2 (R Core Team, 2022) using the 'dplyr' and 'ggplot2' packages for data manipulation and visualization (Wickham, 2016; Wickham et al., 2020). All values are reported as mean \pm one standard deviation unless otherwise indicated. Where

applicable, all statistical models were verified by post-hoc performance assessments to check for normality and heteroscedasticity of residuals.

The effect of chamber transparency on measured CH_4 flux was assessed for each site by a paired sample Wilcoxon signed rank test for individual chamber reps ($n = 15$ paired measurements per site). We evaluated the effect of site on all measured chamber fluxes (pooled CH_4 , NEE from transparent chambers, RECO from opaque chambers) using linear mixed effects models implemented with the "lmer" function in the "lme4" package in R (Bates et al., 2015) with individual chamber replicates as the sample unit ($n = 15$ per site) and site as a fixed effect with month as a random effect to account for repeated measurements. Methane fluxes were log-transformed to meet the assumptions of normality. Contrasts among sites for significant models were conducted via Tukey's honestly significant difference test performed with the "contrasts" function in the "emmeans" R package (Lenth, 2020).

To explore potential drivers of chamber CH_4 and CO_2 fluxes across sites, we computed the mean flux from the three chamber replicates at each site for each date and paired with simultaneously measured (mean values between 10:00 and 14:00 LST on measurements days) environmental variables, including salinity, water-table depth, soil moisture, water temperature, soil temperature, air temperature in the canopy, air temperature above the canopy, relative humidity, and PAR, as well as mean live biomass in the chambers to conduct non-parametric Spearman's rank correlation analysis across all sites and sampling dates ($n = 4 \text{ sites} \times 5 \text{ sampling dates} = 20$). Significant correlation between CH_4 and salinity was further explored with linear regression analysis (Poffenbarger et al., 2011), with CH_4 fluxes log-transformed to conform with assumptions of normality.

We evaluated drivers of CH_4 and CO_2 fluxes using eddy covariance data at the daily scale using univariate ordinary least squares regression. Mean values of soil temperature, water temperature, water-table depth, and salinity across the two chamber sampling sites within the tower footprint at Herring River (*Impounded-Low* and *Impounded-High*), along with air temperature and PAR measured at the tower were used in the models, with CO_2 fluxes (NEE, RECO, and GPP) as drivers of CH_4 flux. We excluded daily values of C fluxes where more than 75% of half-hourly values were gapfilled. Models were constructed for the full annual data set and separately for the growing season only (May–October), since 81% of annual CH_4 was emitted during this period and many of the drivers covaried seasonally (e.g., colder temperatures, higher water table, and higher salinity in the non-growing season). We also assessed the mean diurnal cycle of both NEE and CH_4 flux by averaging fluxes in each half hour of the day binned by month.

To directly compare the instantaneous fluxes measured by the eddy covariance tower with the chamber measurements, we calculated the mean of eddy covariance measurements collected on chamber sampling dates at Herring River between 10:00–14:00 LST when chambers were sampled ($n = 57$ high-quality 30-min flux

measurements) and compared to mean chamber measurements from *Impounded-Low* and *Impounded-High*. We also compared estimates of cumulative CH₄ fluxes from the chambers and measured by the flux tower over the 5-month chamber sampling period (July–November). We scaled chamber CH₄ measurements by converting the instantaneous measurements to the full 24-h period and then developed simple log-linear models based on daily air temperature at each site to estimate daily CH₄ flux from July–November (Figure S4). Although there is substantial uncertainty inherent in upscaling limited measurements to a cumulative seasonal estimate, temperature correcting our measurements (similar to Weston et al., 2014) provided lower, and thus more conservative estimates of CH₄ emission and the associated benefit of tidal restoration than the common assumption that monthly measurements represent a mean monthly flux (Bridgman et al., 2006; Poffenbarger et al., 2011). For the eddy covariance measurements, we summed the gapfilled half-hourly measurements of CH₄ flux for the 5-month period that overlapped with the chamber sampling.

3 | RESULTS

3.1 | Environmental measurements and plant characteristics

The mesohaline sites at the impounded Herring River were consistently fresher and had a higher water table than the polyhaline unrestricted sites at Sage Lot Pond (Figure S5a–d). Salinities at each of the four sites formed a gradient of fresher to more saline from *Impounded-Low* (4.0±0.4 ppt), to *Impounded-High* (8.6±0.8 ppt), to *Unrestricted-Low* (12.0±2.3), to *Unrestricted-High* (24.7±4.8) (Figure S5c,d). At the Herring River sites, water-table depth (where negative values indicate water table below the sediment surface and positive values indicate inundation above the surface) was relatively stable over the growing season and remained near or above the surface, with an average depth of -0.30±1.7 cm (range: -5.3 to +4.0 cm) at *Impounded-Low* and +0.04±1.5 cm (range: -4.2 to +4.4 cm) at *Impounded-High*. Water table at the hydrologically unrestricted Sage Lot Pond sites dropped from June through late September and began to rise again in October, with mean seasonal depth of -13.5±8.4 cm (range: -31.2 to -2.5 cm) at *Unrestricted-Low* and -4.4±7.3 cm (range: -20.4 to +6.8 cm) at *Unrestricted-High* (Figure S5a,b). Water temperature varied seasonally across all sites (Figure S5e,f), with slightly higher mean temperatures at the

unrestricted sites (15.6±2.2°C at *Unrestricted-Low* and 16.7±3.6°C at *Unrestricted-High*) than at the impounded sites (14.6±3.2°C at *Impounded-Low* and 15.1±3.3°C at *Impounded-High*).

Although all sites were dominated by *Phragmites*, the density, height, culm diameter, and total biomass of live vegetation varied significantly (Table 1: linear mixed model: $p < .001$ for all characteristics). Live vegetation was tallest and had the largest diameter at the lowest salinity site (*Impounded-Low*), although the highest culm density was recorded at the highest salinity site (*Unrestricted-High*). The lowest density, height, and culm diameter were found at *Unrestricted-Low*. Total estimated live biomass (dry weight based on both height and culm diameter) scaled by culm density was highest at *Impounded-Low*, followed by comparable values at *Unrestricted-High* and *Impounded-High*, and significantly lower at *Unrestricted-Low* (Table 1).

3.2 | Methane and carbon dioxide fluxes from static chambers

All sites were a measurable source of CH₄ across the season. There was no effect of chamber transparency on measured CH₄ fluxes (Wilcoxon signed rank test: $p \gg .05$ for all sites) at any site (Figure 2a). Therefore, for all subsequent analysis of chamber CH₄ flux we pooled the transparent and opaque measurements. Methane fluxes varied significantly among sites (linear mixed model: marginal $R^2 = .78$, $F = 144.8$, $p < .0001$), with seasonal mean fluxes in descending order of 149.4±76.8 nmolCH₄ m⁻² s⁻¹ at *Impounded-Low*, 68.3±45.1 nmolCH₄ m⁻² s⁻¹ at *Impounded-High*, 20.3±27.3 nmolCH₄ m⁻² s⁻¹ at *Unrestricted-Low*, and 2.8±1.6 nmolCH₄ m⁻² s⁻¹ at *Unrestricted-High* (Figure 2a). On average, there was a 50-fold difference between the sites with the highest and lowest CH₄ flux. Methane fluxes ranked in consistent order of magnitude across sites (*Impounded-Low* > *Impounded-High* > *Unrestricted-Low*, > *Unrestricted-High*) throughout the season and generally declined from higher values in July and August to minima in November (Figure 2b).

We observed potential ebullitive flux of CH₄ for seven light incubations and five dark incubations (11.6% and 8.3% of all measurements, respectively), and there remained no effect of chamber transparency on observed fluxes when potential ebullition was included (Wilcoxon signed rank test: $p \gg .05$ for all sites, Figure S6). All potential ebullition was observed at the impounded sites at Herring River, where both water table and measured CH₄ fluxes were higher

TABLE 1 *Phragmites* characteristics across sites

	Impounded-Low	Impounded-High	Unrestricted-Low	Unrestricted-High
Density (culms m ⁻²)***	27±8 _a	16±3 _b	26±7 _a	54±8 _c
Height (cm)***	410±19 _a	350±2 _b	183±26 _c	228±10 _d
Diameter (mm)***	11±1 _a	8±0.0 _b	5±1 _c	6±0.0 _d
Biomass (kgm ⁻² dry)***	2.2±0.8 _a	0.8±0.1 _b	0.3±0.1 _c	1.0±0.1 _b

*** $p < 0.001$, different letters represent significant contrasts between sites.

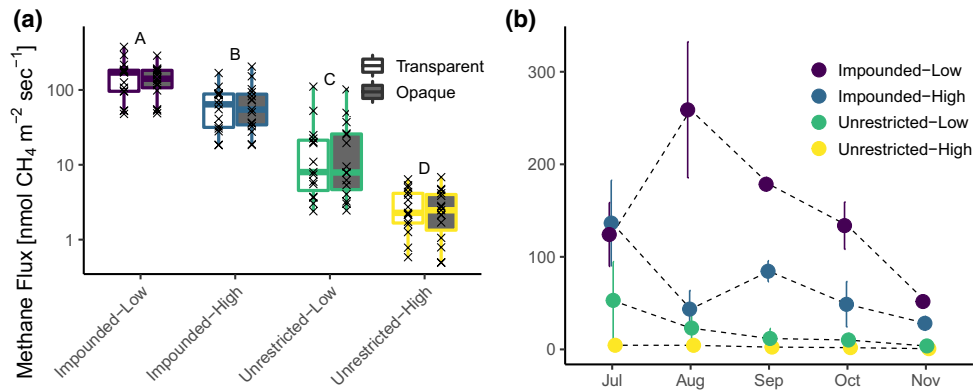


FIGURE 2 (a) Seasonally aggregated methane flux measured from both transparent and opaque chambers at each site. Points represent the individual chamber measurements ($n = 3$ chambers \times 5 sampling events = 15 per subsite), boxes represent the interquartile range, whiskers represent the range excluding outliers, and horizontal bars represent the median. Different letters represent significant contrasts ($p < .05$) among site mean values. Methane flux is displayed on a logarithmic scale along the y-axis to highlight variability in measurements across all sites. (b) Time series of pooled transparent and opaque chamber measurements of methane flux over the five seasonal sampling events. Points represent the mean flux (pooled $n = 2$ chamber transparencies of mean of $n = 3$ chambers) with error bars representing standard deviation. [Colour figure can be viewed at wileyonlinelibrary.com]

than at the unrestricted sites at Sage Lot Pond. Including the potential ebullitive fluxes increased the mean chamber CH₄ measurements by 23% at *Impounded-Low* to 184.5 ± 129.5 nmol CH₄ m⁻² s⁻¹ and by 25% at *Impounded-High* to 85.2 ± 37.3 nmol CH₄ m⁻² s⁻¹ (Figure S6). Although there is evidence of a potentially important contribution of the ebullitive flux pathway to total CH₄ flux at the impounded sites, we cannot estimate the frequency of ebullition nor can we rule out that some of the suspected ebullition we observed was an artifact of our measurement (e.g., disturbance to the soil structure caused by the weight or movement of the chamber). Therefore, we report these values as an upper bound for our flux measurements but omit the ebullitive fluxes from our subsequent analyses.

NEE of CO₂ from the transparent chamber measurements averaged across the season was negative (indicating a carbon sink) at all sites, but flux significantly varied by site (linear mixed model: marginal $R^2 = .24$, $F = 9.8$, $p < .0001$). The greatest NEE flux averaged across the season was -8.1 ± 7.7 $\mu\text{mol CO}_2$ m⁻² s⁻¹ at *Impounded-High*, followed by -4.7 ± 6.0 $\mu\text{mol CO}_2$ m⁻² s⁻¹ at *Impounded-Low*, -1.2 ± 2.1 $\mu\text{mol CO}_2$ m⁻² s⁻¹ at *Unrestricted-Low*, and -0.5 ± 2.5 $\mu\text{mol CO}_2$ m⁻² s⁻¹ at *Unrestricted-High* (Figure 3a). In contrast to CH₄ fluxes, there was some variability in the ranking of NEE magnitude across sites throughout the season (Figure 3b). However, ecosystem respiration of CO₂ measured with the opaque chambers varied more consistently by site (linear mixed model: marginal $R^2 = .12$, $F = 23.7$, $p < .0001$) and reflected the order of magnitude for CH₄ fluxes described above, with highest seasonal mean flux of 8.8 ± 6.0 $\mu\text{mol CO}_2$ m⁻² s⁻¹ at *Impounded-Low* followed by 5.7 ± 4.5 $\mu\text{mol CO}_2$ m⁻² s⁻¹ at *Impounded-High*, with lower and comparable fluxes of 3.9 ± 2.5 $\mu\text{mol CO}_2$ m⁻² s⁻¹ at *Unrestricted-Low* and 3.8 ± 2.4 $\mu\text{mol CO}_2$ m⁻² s⁻¹ at *Unrestricted-High* (Figure 3c). Both NEE and RECO generally followed a seasonal curve with higher magnitudes in July and August and steady decline through senescence in

October and November, with NEE becoming positive (net loss of CO₂ to atmosphere) at all sites in November (Figure 3b,d).

Across all sites and sampling dates, chamber CH₄ flux was positively correlated with chamber RECO, biomass, and PAR, and showed strong negative relationships with NEE (expressed as negative values indicating C uptake into the ecosystem) and salinity (Table 2). Increasing magnitude of NEE and RECO in the chamber were also correlated with increased biomass, PAR, and all measures of temperature and negatively correlated with salinity. The univariate relationship between instantaneous CH₄ chamber flux and salinity across sites was well described by a log-linear regression ($R^2 = .74$, $p < .0001$; Figure 4), but there was no significant effect of salinity within individual sites.

3.3 | Methane and carbon dioxide fluxes from eddy covariance at Herring River

The distribution of continuous CH₄ and CO₂ flux measurements from the eddy covariance tower encompassed the range of fluxes measured by the chambers at the two impounded sites (Figure 5a,b). Average half-hourly flux of CH₄ across the chamber measurement period (June through November) was 46.8 ± 55.1 nmol CH₄ m⁻² s⁻¹ and flux of CO₂ was -1.6 ± 7.8 $\mu\text{mol CO}_2$ m⁻² s⁻¹, while across the entire annual period from May 2020 through May 2021 the mean half-hourly fluxes were 30.1 ± 43.8 nmol CH₄ m⁻² s⁻¹ and -0.9 ± 6.9 $\mu\text{mol CO}_2$ m⁻² s⁻¹. Emission of CH₄ and uptake of CO₂ both displayed a strong seasonal curve that tracked with temperatures (Figure 5c), peaking in late July and with a relatively stable and low flux during the winter from approximately November through April (mean 11.8 ± 11.1 nmol CH₄ m⁻² s⁻¹ and 0.1 ± 5.2 $\mu\text{mol CO}_2$ m⁻² s⁻¹). Across the annual cycle, mean daily fluxes of CH₄ ranged from -0.02 to 0.16 g C m⁻² day⁻¹ with a mean of 0.03 ± 0.03 g C m⁻² day⁻¹ and of

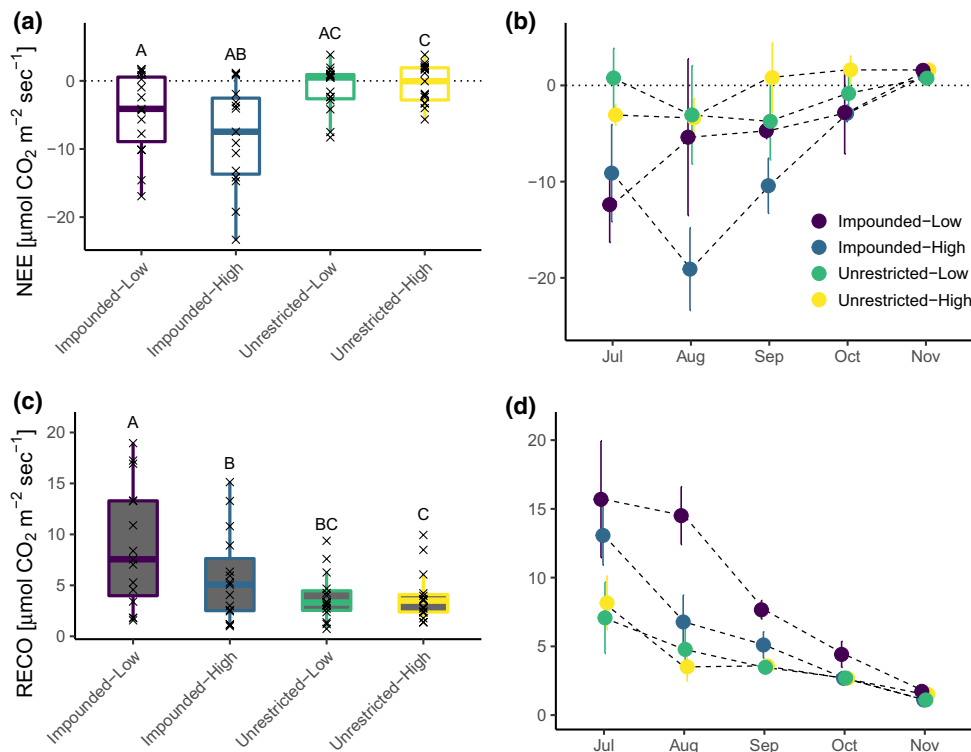


FIGURE 3 Seasonally aggregated (a) net ecosystem exchange (NEE) from transparent and (c) ecosystem respiration (RECO) from opaque chambers at each site. Points represent the individual chamber measurements ($n = 3$ chambers \times 5 sampling events = 15 per subsite), boxes represent the interquartile range, whiskers represent the range excluding outliers, and horizontal bars represent the median. Different letters represent significant contrasts ($p < .05$) among site mean values. Time series of (b) NEE and (d) RECO over the five sampling events. Points represent the mean flux (mean of $n = 3$ chambers) with error bars representing standard deviation. [Colour figure can be viewed at wileyonlinelibrary.com]

CO₂ from -8.28 to -3.87 g C m⁻² day⁻¹ with a mean of -0.96 ± 2.30 g C m⁻² day⁻¹. Total annual emission of CH₄ was 11.4 g C m⁻² (5% = 11.4 g C m⁻²; 95% = 11.3 g C m⁻²) while net annual uptake of CO₂ was -352 g C m⁻² (5% = -389 g C m⁻²; 95% = -321 g C m⁻²).

Along with the expected diurnal cycle of CO₂ flux, there was also a strong diurnal signal in CH₄ flux from the eddy covariance tower with increased CH₄ emissions occurring during the day. The magnitude of the diurnal cycle was highest during the peak of the growing season in July and August, when mid-day flux averaged nearly five-fold higher than nighttime flux, and CH₄ flux was associated with high daytime NEE (Figure 6).

The strongest univariate predictors of daily CH₄ flux across the year were the closely correlated temperature parameters (Figure S7) water temperature ($R^2 = .72$, RMSE = 49.91, $p < .0001$), soil temperature ($R^2 = .71$, RMSE = 48.67, $p < .0001$), and air temperature ($R^2 = .71$, RMSE = 47.76, $p < .0001$). Salinity ($R^2 = .66$, RMSE = 52.13, $p < .0001$), RECO ($R^2 = .58$, RMSE = 47.51, $p < .0001$) and GPP ($R^2 = .48$, RMSE = 47.53, $p < .0001$) were also related to daily CH₄ flux in univariate models, while water-table depth, PAR, NEE, and GPP had significant, but lower explanatory power (Figure S7). Like CH₄, daily NEE was most strongly associated with temperature (air temperature $R^2 = .13$, RMSE = 2.31, $p < .0001$; soil temperature $R^2 = .13$, RMSE = 2.22, $p < .0001$; water temperature $R^2 = .12$, RMSE = 2.25, $p < .0001$), although models for all drivers had weaker explanatory power for NEE

than for CH₄ (Figure S8). When we restricted the analysis to the growing season only, a different set of drivers emerged for CH₄ flux, and overall explanatory power was lower. Similar to the annual analysis, daily growing season CH₄ flux was most strongly related to temperatures, with air temperature as the best predictor ($R^2 = .63$, RMSE = 61.56, $p < .0001$), with slightly lower variability explained by soil temperature ($R^2 = .46$, RMSE = 65.86, $p < .0001$) and water temperature ($R^2 = .31$, RMSE = 69.60, $p < .0001$). Both GPP ($R^2 = .34$, RMSE = 60.98, $p < .0001$) and RECO ($R^2 = .30$, RMSE = 60.99, $p < .0001$) remained relatively strong drivers of CH₄ flux during the growing season (Figure S9). However, salinity ($p = .75$) and water-table depth ($p = .08$), which displayed little variability over the growing season (Figure 5d), had no effect on CH₄ fluxes during this restricted time period.

3.4 | Comparing chamber and eddy covariance measurements for scaling

The two independent and simultaneous flux measurements from the chambers and the tower at Herring River yielded nearly identical mean instantaneous CH₄ emissions over the chamber measurement period (July through November 2020) (Table 3). Measured NEE, however, was reduced by ~40% in the chambers compared to the eddy covariance tower. This difference was driven by both a

TABLE 2 Spearman's rank correlation coefficients among chamber-based methane and carbon dioxide measurements and corresponding environmental variables

	Methane	NEE	RECO	Salinity	Biomass	Water table depth	Soil moisture	Water temp	Soil temp	Canopy temp	Air temp	Relative humidity	PAR
Methane	1												
NEE	-0.59**	1											
RECO	0.64**	-0.74***	1										
Salinity	-0.89***	0.50*	-0.48*	1									
Biomass	0.62**	-0.76***	0.79***	-0.52*	1								
Water table depth	0.44	-0.27	0.07	-0.33	0.35	1							
Soil moisture	0.23	-0.32	0.45*	-0.01	0.56*	0.49*	1						
Water temp	0.04	-0.51*	0.69***	0.16	0.4	-0.19	0.39	1					
Soil temp	0.04	-0.52*	0.71***	0.14	0.4	-0.23	0.39	0.98***	1				
Canopy temp	0.27	-0.57**	0.82***	-0.06	0.46*	-0.12	0.50*	0.89***	0.91***	1			
Air temp	0.29	-0.54*	0.79***	-0.08	0.43	-0.07	0.54*	0.85***	0.86***	0.96***	1		
Relative humidity	-0.1	0.26	-0.34	-0.03	-0.29	0.16	-0.13	-0.24	-0.24	-0.22	-0.08	1	
PAR	0.47*	-0.46*	0.74***	-0.26	0.57**	-0.06	0.51*	0.50*	0.51*	0.62**	0.57**	-0.68***	1

*** $p < 0.001$; ** $p < 0.01$; * $p < 0.05$.

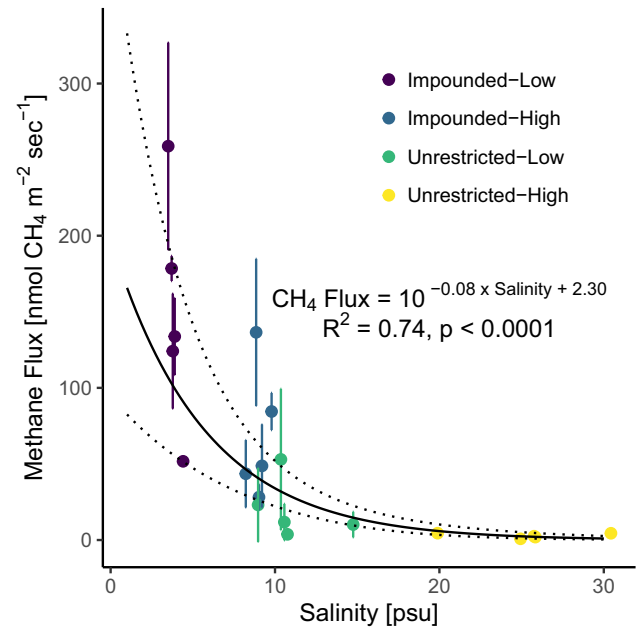


FIGURE 4 Chamber-based methane flux as a function of salinity across all sites and sampling dates. Error bars represent standard deviation of mean methane flux ($n = 3$). The solid line is the univariate log-linear regression model and the dotted lines represent the 95% confidence interval. [Colour figure can be viewed at wileyonlinelibrary.com]

~45% increase in RECO and a 12% decrease in GPP in the chambers relative to eddy covariance measurements. Scaled to a cumulative CH_4 emissions estimate for the 5-month chamber sampling period from July–November, the eddy covariance measurement, which integrates day and night fluxes, was 56% lower than the chamber-based estimate from *Impounded-Low* and 5% lower than the estimate from *Impounded-High*, with a 40% reduction overall compared to the mean estimate from both impounded chamber sites (Table 4).

4 | DISCUSSION

Carbon cycling in the diked and impounded ecosystems that represent a significant portion of coastal wetland areas is poorly characterized and a potentially valuable blue carbon opportunity via tidal restoration to reduce CH_4 emissions (Kroeger et al., 2017). Our study was designed to investigate CH_4 and CO_2 flux across a salinity range spanning impounded and unrestricted coastal wetlands dominated by *Phragmites* to better understand the influence of salinity in a vegetation stratum that commonly occurs in impounded wetland ecosystems. Like prior syntheses that encompass a range of wetland vegetation types (Poffenbarger et al., 2011; Windham-Myers et al., 2018), we found that flux of CH_4 increases exponentially as salinity decreases across *Phragmites* wetlands. Thus, our results provide what may be a first critical confirmation that resalinization could dramatically reduce CH_4 emission in impounded ecosystems dominated by *Phragmites*. We also used eddy covariance to collect continuous measurements of C gas exchange from a freshened, impounded estuary, to our knowledge the first such data set of its kind.

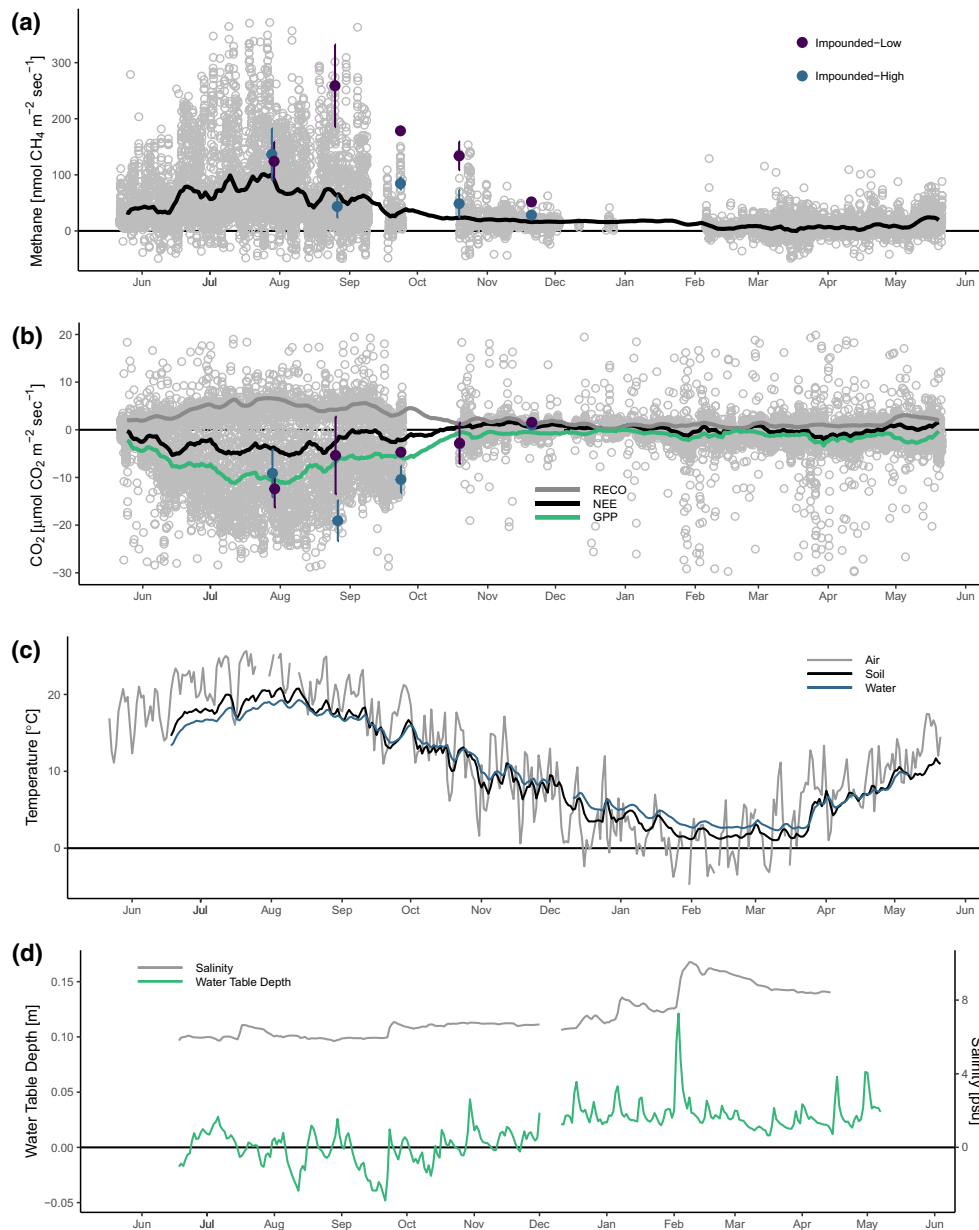


FIGURE 5 Measured eddy covariance fluxes of (a) methane and (b) net ecosystem exchange (NEE) of carbon dioxide at the Herring River impounded wetland from May through November 2020. Gray points show individual, high-quality half-hourly NEE measurements and the black line represents a 5-day running mean of gapfilled daily fluxes of NEE, along with a similar 5-day running mean of ecosystem respiration (RECO) and gross primary production (GPP). Chamber measurements with standard deviation error bars from within the tower footprint at *Impounded-low* and *Impounded-high* are plotted for comparison. (c) Mean daily air temperature measured at the flux tower with soil and water temperature, along with (d) water-table depth relative to sediment surface and salinity presented as the mean values recorded at *Impounded-high* and *Impounded-low*. [Colour figure can be viewed at [wileyonlinelibrary.com](https://onlinelibrary.wiley.com)]

This site is a strong and continuous source of CH_4 and a powerful CO_2 sink. We observed little variation in salinity and water-table depth during the growing season because of disconnected and impounded hydrology, and consequently soil temperature was the strongest predictor of both CH_4 and CO_2 fluxes. The continuous eddy covariance measurements allowed us to observe a strong diurnal signal in CH_4 flux, which has important methodological implications for measuring and scaling CH_4 fluxes from similar ecosystems for blue carbon crediting applications.

4.1 | Salinity is a strong control on C exchange in *phragmites* wetlands

The widespread observation that CH_4 emissions are higher in wetlands with lower salinity (Bartlett et al., 1987; Martin & Moseman-Valtierra, 2015; Poffenbarger et al., 2011; Wang et al., 2017; Windham-Myers et al., 2018) was upheld in our study across four *Phragmites* wetland sites ranging from ~4 to 25 psu. The nearly 50-fold

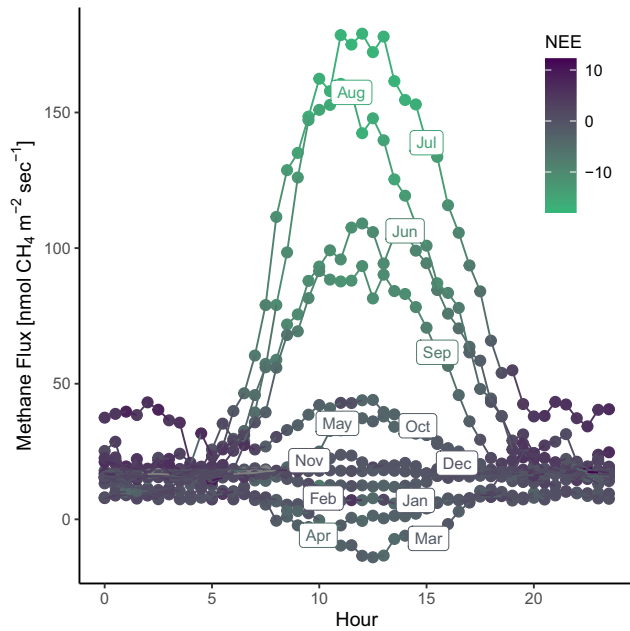


FIGURE 6 Diurnal variation of half-hourly CH_4 flux measured via eddy covariance at Herring River binned by month. The color scale indicates corresponding mean net ecosystem exchange in $\mu\text{mol CO}_2 \text{ m}^{-2} \text{ s}^{-1}$. [Colour figure can be viewed at wileyonlinelibrary.com]

TABLE 3 Comparison of mean eddy covariance and static chamber (*Impounded-low* and *Impounded-high*) measurements of instantaneous carbon flux measured simultaneously (between 10:00 and 14:00 local standard time on sampling days) at the impounded Herring River

	Eddy covariance	Chambers
CH_4 -midday [$\text{nmol m}^{-2} \text{ s}^{-1}$]	111.9 ± 72.3	111.5 ± 83.6
NEE-midday [$\mu\text{mol m}^{-2} \text{ s}^{-1}$]	-10.6 ± 6.2	-6.4 ± 7.0
RECO-midday [$\mu\text{mol m}^{-2} \text{ s}^{-1}$]	5.0 ± 3.0	7.3 ± 5.4
GPP-midday [$\mu\text{mol m}^{-2} \text{ s}^{-1}$]	-15.5 ± 8.8	-13.7 ± 10.7

difference (excluding ebullition) in mean CH_4 flux from the freshest impounded site to the most saline tidally unrestricted site supports the idea that increased salinization of impounded *Phragmites* wetlands could dramatically reduce CH_4 emission (Kroeger et al., 2017). The relationship between salinity and CH_4 emission has been attributed to sulfate reduction predominating anaerobic C respiration when sulfate is abundant in high salinity ecosystems, whereas methanogenesis becomes more prevalent in freshwater systems where sulfate is limited (Luo et al., 2019; Weston et al., 2006).

Salinity covaried with both biomass and water-table depth, which complicates the observed salinity effect on CH_4 flux. Increased *Phragmites* biomass and a trend of more rapid CO_2 cycling (greater rates of both NEE and RECO) at the fresher impounded sites with a negative correlation of CO_2 cycling with increased salinity reflects the well documented sensitivity of *Phragmites* to saline conditions (Burdick

TABLE 4 Cumulative CH_4 emission from July–November 2020 based on scaled temperature-modeled chamber measurements at each site, along with mean values across the two chamber sites at the impounded Herring River (*Impounded* [mean]) representing the footprint of the eddy covariance tower. The ratio of cumulative CH_4 measured via eddy covariance and the mean of impounded chambers was used to develop a vegetation-specific scaling factor of 0.6 to account for the diurnal cycling of CH_4 in *Phragmites* ecosystems. In addition, the ratio of July–Nov cumulative CH_4 emissions to annual CH_4 emissions (11.4 g C m^{-2}) at the eddy covariance tower (-1.2) was used to scale chamber values to an annualized CH_4 flux. All values are expressed as g C m^{-2} , except as indicated where CH_4 flux was converted to CO_2 equivalents based on sustained flux global warming potential (Neubauer & Megonigal, 2015) for contextualization

	Cumulative chamber scaled CH_4 flux (Jul–Nov) [$\text{g CH}_4 \text{ C m}^{-2} \text{ year}^{-1}$]	Cumulative eddy covariance CH_4 flux (July–Nov) [$\text{g CH}_4 \text{ C m}^{-2} \text{ year}^{-1}$]	Annualized chamber CH_4 flux scaled by ratio of measurement period to annual eddy covariance cumulative estimate (1.2) [$\text{g CH}_4 \text{ C m}^{-2} \text{ year}^{-1}$]	Annualized chamber CH_4 flux with <i>phragmites</i> scaling factor (0.6) [$\text{g CH}_4 \text{ C m}^{-2} \text{ year}^{-1}$]	CO_2 equivalent annualized and scaled chamber CH_4 flux [$\text{g CO}_2 \text{ eq m}^{-2} \text{ year}^{-1}$]
Impounded-Low	21.3	25.6	25.6	15.3	922
Impounded-High	9.7	11.6	11.6	7.0	420
Unrestricted-Low	3.4	4.1	4.1	2.4	147
Unrestricted-High	0.4	0.5	0.5	0.3	17
Impounded (mean)	15.5	18.6	18.6	11.2	671

et al., 2001; Chambers et al., 2003; Schenck et al., 2018; Vasquez et al., 2006) and suggests that primary production is enhanced with reduced salinity across the gradient. More labile C availability at fresher sites where productivity is high likely stimulates CH₄ production (Hatala et al., 2012; Kim, Chaudhary, et al., 2020; Mozdzer & Megonigal, 2013; Van Der Nat & Middelburg, 1998). Higher biomass could also increase CH₄ emission due to the enhancement of plant-mediated conduction of CH₄ to the atmosphere (Van Der Nat & Middelburg, 1998). While the data available from our current study do not allow us to tease out the relative contribution of sulfate availability, C availability, and plant-mediated gas transport on the salinity effect on CH₄ emissions, we posit that within *Phragmites* wetlands these factors are likely to predictably covary. However, the covariation of water-table depth and salinity in our study is probably less universal and an artifact of the individual sites selected. Since higher water table is linked to increased CH₄ emission (e.g., Evans et al., 2021), we cannot rule out higher water level as a driver of some of the higher CH₄ fluxes that we observed across our salinity gradient, even though the effect of water table was not significant here.

The CH₄ emission values presented in our analysis potentially underestimate the difference between the low and high end of the salinity gradient due to exclusion of ebullition events and moderate drought conditions during the study period. Incorporating potential observed ebullition events increases the mean flux rate measured by our chambers at the fresher impounded sites by approximately 25%, leads to greater variation of CH₄ flux in our data set at the low end of the salinity range, and enhances the differences in CH₄ measured across the salinity gradient. However, our sampling was not designed to estimate the frequency and, therefore, importance of this pathway. Prior studies have demonstrated that in dense, emergent wetland vegetation like *Phragmites*, CH₄ flux from ebullition is much less significant than the plant mediated flux (van den Berg et al., 2020). Further, given the moderate to increasingly severe drought conditions experienced across our sites during the study year (USDM, 2021), our measurements may not be reflective of mean conditions at these locations. Monitoring data at the Herring River from 2017–2019 (O'Keefe Suttles et al., 2020) indicate a slightly higher water level and lower salinity in prior years, while monitoring data collected near the *Unrestricted-High* site at Sage Lot Pond (O'Keefe Suttles, Eagle, Martin, et al., 2022) also point to higher water table and lower salinity in years without drought. Given the importance of salinity demonstrated in our study and the general importance of water level for CH₄ emissions (Evans et al., 2021), we speculate that the dry and relatively saline conditions in 2020 may have suppressed CH₄ emission across the gradient relative to more typical years.

4.2 | Brackish, impounded coastal wetland is a strong sink for CO₂, source for CH₄

The annual NEE of $-352\text{ gCO}_2\text{-Cm}^{-2}\text{ year}^{-1}$ and CH₄ emission of $11.4\text{ gCH}_4\text{-Cm}^{-2}\text{ year}^{-1}$ measured by the eddy covariance tower at the Herring River indicate that this impounded ecosystem is a strong sink for CO₂ but also an important source of CH₄. We note

that unlike our chamber-based measurements, the eddy covariance measurements do incorporate CH₄ fluxes from ebullition. Although limited comparable eddy covariance measurements exist in this geographical region, our values suggest a high CO₂ uptake via NEE relative to the $-179\pm 32\text{ gCm}^{-2}\text{ year}^{-1}$ reported for a natural tidal salt marsh in northern Massachusetts (Forbrich et al., 2018), $-213\text{ gCm}^{-2}\text{ year}^{-1}$ for a restored tidal marsh (Artigas et al., 2015) and $-73\text{ gCm}^{-2}\text{ year}^{-1}$ (Schäfer et al., 2019) for a natural tidal marsh in New Jersey, and $138\pm 108\text{ gCm}^{-2}\text{ year}^{-1}$ emission for a tidal salt marsh in Delaware (Vázquez-Lule & Vargas, 2021), while globally averaged NEE for coastal wetlands measured by eddy covariance has been reported at $-208\pm 89\text{ gCm}^{-2}\text{ year}^{-1}$ (Lu et al., 2017). Although eddy covariance data on CH₄ exchange in coastal marshes remains limited, the CH₄ emissions from this site far exceed the median salt marsh emissions of $0.8\pm 2.9\text{ gCm}^{-2}\text{ year}^{-1}$ recently reported from a global synthesis (Knox et al., 2019), but the value is comparable to the $11.1\pm 3.6\text{ gCm}^{-2}\text{ year}^{-1}$ reported for a mesohaline salt marsh in Delaware (Vázquez-Lule & Vargas, 2021) and $11\text{ gCm}^{-2}\text{ year}^{-1}$ for a brackish marsh in coastal Louisiana (Krauss et al., 2016).

The total CH₄ emission measured from this ecosystem is about 59% higher than the $7.2\text{ gCm}^{-2}\text{ year}^{-1}$ that would be predicted from the model developed by Poffenbarger et al. (2011) based on annual site salinity (7.1 psu). This is due in part to the high uncertainty at the low end of the salinity range for that model (Poffenbarger et al., 2011). It may also suggest that salinity alone is not a sufficient proxy for CH₄ emissions in impounded ecosystems. When hydrologic flushing is restricted, it is possible that sulfate consumption without tidal replenishment leads to an even higher degree of sulfate depletion than would be indicated by salinity measurements (Koebsch et al., 2019). Incorporating additional parameters, like sulfate concentrations, water-table depth, and vegetation type and biomass may be needed to develop a model that can better predict annual CH₄ exchange in impounded ecosystems.

Daily variation in both CH₄ and CO₂ fluxes across the year were well explained by water temperature, and the closely related parameters of air and soil temperatures, with air temperature strongly predominating in the growing season. The dominant control of CH₄ and CO₂ fluxes by temperature aligns with previous findings across a range of coastal wetlands (Abdul-Aziz et al., 2018). Since the site does not experience wide variation in salinity or water-table depth during the growing season because of the managed hydrology, the importance of these parameters in driving daily CH₄ flux is dramatically reduced during the growing season when CH₄ fluxes are at their peak. The low variability in the key parameters of salinity and water-table depth are likely to be characteristic of impounded ecosystems and therefore it is important to consider the elevated importance of temperature as a driver of CH₄ flux for modeling emissions.

4.3 | Diurnal cycle requires consideration when scaling CH₄ measurements

Despite the strong agreement between synchronous flux measurements via static chambers and eddy covariance (Table 3), the diurnal

cycle in CH_4 exchange that we observed signals that caution is warranted for scaling chamber-based CH_4 fluxes to daily, monthly, or annual values. By assuming that our mid-day measurements represent a constant daily CH_4 flux, we would overestimate cumulative CH_4 emission during the 5-month chamber sampling period relative to the eddy covariance estimate by roughly 70% (Table 4). At the scale of a blue carbon crediting project, this error is tremendously important. Yet, this kind of extrapolation is currently permitted in C accounting methodology (Needleman et al., 2018) and has been incorporated into global syntheses of CH_4 emission in coastal wetlands (Al-Haj & Fulweiler, 2020; Poffenbarger et al., 2011; Windham-Myers et al., 2018).

A diurnal cycle in CH_4 flux has been widely documented in other *Phragmites* ecosystems (Duan et al., 2005; van den Berg et al., 2016, 2020), as well as those dominated by rice, cattail, and *Scirpus* (Hatala et al., 2012; Van Der Nat et al., 1998; Villa et al., 2020). Researchers have attempted to capture the diurnal cycle by pairing mid-day transparent and opaque chamber measurements to simulate nighttime fluxes and unlike in our study, some have observed a positive effect of light on CH_4 emission (Hirota et al., 2007; Moseman-Valtierra et al., 2016; Van der Nat & Middelburg, 2000). However, we speculate that our shorter incubations (3–7 min vs. 30–40 min in some of these prior studies), which minimize artifacts like chamber heating and dramatic changes in CO_2 and CH_4 concentrations during sampling, do not allow enough time for physiological adaptation (e.g., stomatal closure) to dark conditions to observe a simulated nighttime effect. Therefore, this approach seems inconsistent and likely fails to capture the actual nighttime effect.

The mechanism for the daytime peak in CH_4 emission is likely associated with plant-mediated transport, driven by a pressure gradient that is stronger during active photosynthesis (Armstrong & Armstrong, 1991; van den Berg et al., 2020). Previous studies have also linked mid-day peaks in CH_4 production to an abundance of newly fixed carbon substrate for methanogenesis (Hatala et al., 2012) and diel variations in soil temperature (Bansal et al., 2018). These mechanisms are not mutually exclusive and may all be factors in the pattern we observe here. In this *Phragmites* dominated ecosystem, the diurnal effect is relatively large (daytime fluxes of CH_4 up to five times higher than nighttime fluxes). Other types of ecosystems dominated by vegetation with weaker plant-mediated flux may have little or no diurnal variation in CH_4 emission.

Further research to characterize the relative importance of diurnal cycling in CH_4 flux across different types of vegetation could help inform appropriate monitoring strategies for blue carbon projects. We propose that when feasible, CH_4 flux measurements be collected over a 24-h cycle, either with chambers or eddy covariance, since brief dark daytime chamber measurements did not capture the diurnal effect in our study. However, daytime chamber measurements represent the vast majority of the data we have available on CH_4 fluxes from tidal wetlands (Al-Haj & Fulweiler, 2020; Poffenbarger et al., 2011; Windham-Myers et al., 2018) and are likely to remain dominant given the financial and logistical constraints of conducting 24-h sampling. Therefore, determining the most appropriate way

to scale these data is critical. Vegetation specific scaling factors for daytime chamber measurements would allow for the continuation of convenient daytime monitoring to be applied.

We can use the relationship between cumulative estimates from both flux measurement methods in our study to develop a scaling factor appropriate to CH_4 emission patterns of *Phragmites*. Over the 5-month chamber sampling period, the cumulative CH_4 emission measurement from the eddy covariance tower at Herring River (9.2 g C m^{-2}) is less than the mean of the estimates from the two chamber sites at Herring River for the same period (15.5 g C m^{-2} ; Table 4). If we assume that the mean of the two sampling sites at Herring River (*Impounded-Low* and *Impounded-High*, both dominated by *Phragmites*) roughly represent the footprint of the eddy covariance tower (Figure S1), calculate the ratio of the two measures of cumulative CH_4 emission, we get a *Phragmites*-specific scaling factor of ~ 0.6 to apply to mid-day chamber measurements to account for the diurnal cycle.

To scale up our chamber measurement period to a full annual cycle, we used the ratio of our measured annual estimate of CH_4 emission from the eddy covariance tower (11.4 g C m^{-2}) compared to the July–November cumulative emission measured during the chamber sampling period (9.2 g C m^{-2}) to derive a factor of ~ 1.2 to apply to July–November cumulative chamber values. This approach to scaling shorter term measurements to annualized fluxes is similar to the scaling method developed by Bridgman et al. (2006) and used by Poffenbarger et al. (2011) to convert daily growing season measurements to a full annual cycle. By applying these two scaling factors (that is, our primary recommendation of the vegetation-specific scaling factor to account for diurnal cycle of CH_4 emissions and the annualized scaling factor required due to the timing of this study), we can estimate annual CH_4 emission values across our salinity gradient (Table 4). While there is error associated with this rough scaling approach, using this method or other related strategies to account for the well documented diurnal cycle of CH_4 flux in many types of wetland vegetation (Duan et al., 2005; Hatala et al., 2012; van den Berg et al., 2016, 2020; Van Der Nat & Middelburg, 1998; Villa et al., 2020) could avoid substantial errors in scaling that lead to overestimation of baseline CH_4 for carbon credit quantification, planning, and monitoring applications.

4.4 | Implications for radiative balance and blue carbon management potential of impounded *Phragmites* coastal ecosystems

To assess the radiative impact of the CH_4 emission from the impounded Herring River, we calculated the sustained flux global warming potential over 100 years (Neubauer & Megonigal, 2015) of the annual CH_4 emission measured in our study against the C accumulation rate at this site ($-630 \text{ g CO}_2\text{-eq m}^{-2} \text{ year}^{-1}$, O'Keefe Suttles, Eagle, Mann, Wang, et al., 2021). We use C accumulation rate, which represents the newly fixed C that remains sequestered in the wetland, rather than NEE, to

TABLE 5 Sustained flux global warming potential of CH₄ emission to the atmosphere and C accumulation over a 100-year time frame. All values are reported in gCO₂-equivalents m⁻² year⁻¹

	CH ₄	CO ₂	Net	CH ₄ data source	C accumulation data source
Impounded Phragmites, Herring River	685	-630	55	This study, eddy covariance	O'Keefe Suttles, Eagle, Mann, Wang, et al. (2021)
Unrestricted Phragmites, Sage Lot Pond	84	-491	-408	This study, mean chambers	O'Keefe Suttles, Eagle, Martin, et al. (2022)
Unrestricted Spartina, Cape Cod North Shore	48	-986	-938	Knox et al. (2019)	O'Keefe Suttles, Eagle, Mann, Spivak, et al. (2021)

account for the up to 50% of NEE that may be exported from the marsh platform via lateral flow (Bogard et al., 2020; Wang et al., 2016). Over this timeframe, the CH₄ emissions at the impounded Herring River site completely offset the C storage and give this ecosystem a positive net radiative balance (Table 5).

Resalinization of impounded *Phragmites* wetlands with restoration of tidal flow would push ecosystems towards the more saline end of our gradient and reduce CH₄ emission. Although *Phragmites* tends to be less competitive in more saline conditions, established populations can persist despite increased salinity (Hazelton et al., 2014). Therefore, saline conditions would also likely reduce primary production, as indicated by the decreased *Phragmites* biomass and NEE at the unrestricted sites reported here and supported by C accumulation rate measured in the *Phragmites* zone at the unrestricted Sage Lot Pond site (-491 gCO₂-eq m⁻², O'Keefe Suttles, Eagle, Martin, et al., 2022). Based on the mean CH₄ emission value from the two unrestricted sites at Sage Lot Pond (1.3 gC m⁻² year⁻¹, from Table 4), the reduction in CH₄ emission with tidal restoration would likely compensate for the reduced productivity and result in an ecosystem with a strong net negative radiative balance (Table 5). Ultimately though, restoration of saline tidal flow to an impounded site like the Herring River, if coupled with active *Phragmites* removal to enable reestablishment of native vegetation, should result in a restored natural salt marsh ecosystem. Applying the same sustained flux global warming potential and assuming recovery of C storage to the rate observed in a natural analog to the Herring River dominated by *Spartina* on the north shore of Cape Cod (-986 gCO₂-eq m⁻² year⁻¹; O'Keefe Suttles, Eagle, Mann, Spivak, et al., 2021) and CH₄ emission of 0.8 gC m⁻² year⁻¹ based on the median value for salt marsh ecosystems (Knox et al., 2019), we could expect the restored radiative balance of this ecosystem to be on the order of -938 gCO₂-eq m⁻² year⁻¹ (Table 5). This suggests that restoration of tidal flow accompanied by active management strategies to remove *Phragmites* and replace with native salt marsh vegetation can be twice as effective as resalinization alone. Over the entire *Phragmites*-dominated stratum of the Herring River ecosystem (about 21 ha), full restoration from the current impounded state to a salt marsh ecosystem could avoid emission of 208 metric tonnes CO₂-eq year⁻¹ from just one subset of the ~400 ha estuary. Excluding the effects of sea-level rise and climate change, as well as the transition phase of the

restoration that would lead to a transient net emission of CO₂ from biomass turnover, this could result in a net mitigation of 4160 metric tonnes of CO₂-eq over 20 years.

When considered within time horizons relevant to meeting the global Paris Agreement target of limiting warming to 1.5°C above pre-industrial levels (United Nations, 2015), it has been suggested that the global warming potential of CH₄ be revised to 75 times that of CO₂ (Abernethy & Jackson, 2022), which would result in a 40% increase in the calculated benefit of the Herring River restoration. Although questions remain as to the net climate benefit of conserving many existing blue carbon ecosystems due to poorly constrained CH₄ and nitrous oxide emissions that can offset C sequestration (Rosentreter et al., 2021), this study suggests that restoration of saline tidal flow would predictably reduce CH₄ emission and provide reliable carbon offsets.

5 | CONCLUSIONS

We empirically demonstrate that in impounded coastal wetlands dominated by *Phragmites*, salinization with tidal restoration can markedly reduce CH₄ emission, an effective blue carbon opportunity and key information for decision-makers and stakeholders to manage GHG emissions. Pairing multiple measurement techniques was a powerful approach to learn about important drivers of CH₄ in these understudied ecosystems and resulted in management-relevant recommendations for scaling and monitoring, namely attention to the diurnal cycle of CH₄ flux and the elevated importance of temperature, that are key to ensuring accurate baseline and restoration assessments for blue carbon applications in impounded ecosystems. While challenges remain for widespread implementation of coastal wetland restoration in a natural climate solutions framework, this study provides an improved understanding of C exchange in impounded ecosystems that will help advance this critical agenda.

ACKNOWLEDGMENTS

This project was supported by USGS-NPS Natural Resources Preservation Program #2021-07, U.S. Geological Survey Coastal

& Marine Hazards and Resources Program and the USGS Land Change Science Program's LandCarbon program, and NOAA National Estuarine Research Reserve Science Collaborative NA14NOS4190145. R Sanders-DeMott was supported by a USGS Mendenhall Fellowship and partnership with Restore America's Estuaries. We also acknowledge our stakeholder partners, including the Cape Cod National Seashore, Waquoit Bay National Estuarine Research Reserve, Friends of Herring River, and the Bringing Wetlands to Market project team, along with Thomas Mozdzer and Eric Marsjanik for technical assistance with chamber design. Any use of trade, firm or product names is for descriptive purposes only and does not imply endorsement by the U.S. Government.

CONFLICT OF INTEREST

The authors declare that there is no conflict of interest.

DATA AVAILABILITY STATEMENT

The data that support the findings of this study are available from Sanders-DeMott et al. (2022); <http://doi.org/10.5066/P9RRL3TO> and O'Keefe Suttles, Eagle, Sanders-DeMott, et al. (2022); <https://doi.org/10.5066/P9T1KOTW>.

ORCID

Rebecca Sanders-DeMott  <https://orcid.org/0000-0002-0709-8042>

Meagan J. Eagle  <https://orcid.org/0000-0001-5072-2755>

Kevin D. Kroeger  <https://orcid.org/0000-0002-4272-2349>

Faming Wang  <https://orcid.org/0000-0002-7543-6779>

Thomas W. Brooks  <https://orcid.org/0000-0002-0555-3398>

Jennifer A. O'Keefe Suttles  <https://orcid.org/0000-0003-2345-5633>

Sydney K. Nick  <https://orcid.org/0000-0003-4901-7308>

Adrian G. Mann  <https://orcid.org/0000-0003-1689-8524>

Jianwu Tang  <https://orcid.org/0000-0003-2498-9012>

REFERENCES

- Abdul-Aziz, O. I., Ishtiaq, K. S., Tang, J., Moseman-Valtierra, S., Kroeger, K. D., Gonneea, M. E., Mora, J., & Morkeski, K. (2018). Environmental controls, emergent scaling, and predictions of greenhouse gas (GHG) fluxes in coastal salt marshes. *Journal of Geophysical Research: Biogeosciences*, 123(7), 2234–2256. <https://doi.org/10.1029/2018JG004556>
- Abernethy, S., & Jackson, R. B. (2022). Global temperature goals should determine the time horizons for greenhouse gas emission metrics. *Environmental Research Letters*, 17(2), 024019. <https://doi.org/10.1088/1748-9326/ac4940>
- Al-Haj, A. N., & Fulweiler, R. W. (2020). A synthesis of methane emissions from shallow vegetated coastal ecosystems. *Global Change Biology*, 26(5), 2988–3005. <https://doi.org/10.1111/gcb.15046>
- Arguez, A., Durre, I., Applequist, S., Vose, R. S., Squires, M. F., Yin, X., Heim, R. R., Jr., & Owen, T. W. (2012). NOAA's 1981-2010 climate normals: An overview. *Bulletin of the American Meteorological Society*, 93, 1687–1697.
- Armstrong, J., & Armstrong, W. (1991). A convective through-flow of gases in *Phragmites australis* (Cav.) Trin. Ex Steud. *Aquatic Botany*, 39(1–2), 75–88. [https://doi.org/10.1016/0304-3770\(91\)90023-X](https://doi.org/10.1016/0304-3770(91)90023-X)
- Armstrong, J., Jones, R. E., & Armstrong, W. (2006). Rhizome phyllosphere oxygenation in phragmites and other species in relation to redox potential, convective gas flow, submergence and aeration pathways. *New Phytologist*, 172(4), 719–731. <https://doi.org/10.1111/j.1469-8137.2006.01878.x>
- Artigas, F., Shin, J. Y., Hobbie, C., Marti-Donati, A., Schäfer, K. V. R., & Pechmann, I. (2015). Long term carbon storage potential and CO₂ sink strength of a restored salt marsh in New Jersey. *Agricultural and Forest Meteorology*, 200, 313–321. <https://doi.org/10.1016/j.agrformet.2014.09.012>
- Aubinet, M. (2008). Eddy covariance CO₂ flux measurements in nocturnal conditions: An analysis of the problem. *Ecological Applications*, 18(6), 1368–1378. <https://doi.org/10.1890/06-1336.1>
- Baldocchi, D. D. (2003). Assessing the Eddy covariance technique for evaluating the carbon balance of ecosystems. *Global Change Biology*, 9(2002), 1–41.
- Bansal, S., Tangen, B., & Finocchiaro, R. (2018). Diurnal patterns of methane flux from a seasonal wetland: Mechanisms and methodology. *Wetlands*, 38(5), 933–943. <https://doi.org/10.1007/s13157-018-1042-5>
- Bartlett, K. B., Bartlett, D. S., Harriss, R. C., & Sebacher, D. I. (1987). Methane emissions along a salt marsh salinity gradient. *Biogeochemistry*, 4(3), 183–202. <https://doi.org/10.1007/BF02187365>
- Bates, D., Machler, M., Bolker, B., & Walker, S. (2015). Fitting linear mixed-effects models using {lme4}. *Journal of Statistical Software*, 67(1), 1–48. <https://doi.org/10.18637/jss.v067.i01>
- Bogard, M. J., Bergamaschi, B. A., Butman, D. E., Anderson, F., Knox, S. H., & Windham-Myers, L. (2020). Hydrologic export is a major component of coastal wetland carbon budgets. *Global Biogeochemical Cycles*, 34(8), 1–14. <https://doi.org/10.1029/2019GB006430>
- Bridgman, S. D., Magonigal, J. P., Keller, J. K., Bliss, N. B., & Trettin, C. (2006). The carbon balance of North American wetlands. *Wetlands*, 26(4), 889–916. [https://doi.org/10.1672/0277-5212\(2006\)26\[889:TCBONA\]2.0.CO;2](https://doi.org/10.1672/0277-5212(2006)26[889:TCBONA]2.0.CO;2)
- Burba, G. G., McDermitt, D. K., Grelle, A., Anderson, D. J., & Xu, L. (2008). Addressing the influence of instrument surface heat exchange on the measurements of CO₂ flux from open-path gas analyzers. *Global Change Biology*, 14(8), 1854–1876. <https://doi.org/10.1111/j.1365-2486.2008.01606.x>
- Burdick, D. M., Buchsbaum, R., & Holt, E. (2001). Variation in soil salinity associated with expansion of *Phragmites australis* in salt marshes. *Environmental and Experimental Botany*, 46(3), 247–261. [https://doi.org/10.1016/S0098-8472\(01\)00099-5](https://doi.org/10.1016/S0098-8472(01)00099-5)
- Chambers, R. M., Osgood, D. T., Bart, D. J., & Montalto, F. (2003). *Phragmites australis* invasion and expansion in tidal wetlands: Interactions among salinity, sulfide, and hydrology. *Estuaries*, 26(2), 398–406. <https://doi.org/10.1007/BF02823716>
- Chmura, G. L., Anisfeld, S. C., Cahoon, D. R., & Lynch, J. C. (2003). Global carbon sequestration in tidal, saline wetland soils. *Global Biogeochemical Cycles*, 17(4), 1111. <https://doi.org/10.1029/2002GB001917>
- Christoffersen, B. (2019). *rollRegres: Fast rolling and expanding window linear regression*. R package version 0.1.3. <https://cran.r-project.org/package=rollRegres>
- Clean Energy Regulator. (2022). Tidal restoration of blue carbon ecosystems method. <http://www.cleanenergyregulator.gov.au/ERF/Choosing-a-project-type/Opportunities-for-the-land-sector/Vegetation-methods/tidal-restoration-of-blue-carbon-ecosystems-method>
- Crooks, S., Sutton-Grier, A. E., Troxler, T. G., Herold, N., Bernal, B., Schile-Beers, L., & Wirth, T. (2018). Coastal wetland management as a contribution to the US National Greenhouse gas Inventory. *Nature Climate Change*, 8(12), 1109–1112. <https://doi.org/10.1038/s41558-018-0345-0>
- Davidson, E. A., Belk, E., & Boone, R. D. (1998). Soil water content and temperature as independent or confounded factors controlling soil respiration

- in a temperate mixed hardwood forest. *Global Change Biology*, 4(2), 217–227. <https://doi.org/10.1046/j.1365-2486.1998.00128.x>
- DeLaune, R. D., Smith, C. J., & Patrick, W. H. (1983). Methane release from gulf coast wetlands. *Tellus B: Chemical and Physical Meteorology*, 35(1), 8–15. <https://doi.org/10.3402/tellusb.v35i1.14581>
- Duan, X., Wang, X., Mu, Y., & Ouyang, Z. (2005). Seasonal and diurnal variations in methane emissions from Wuliangsu Lake in arid regions of China. *Atmospheric Environment*, 39(25), 4479–4487. <https://doi.org/10.1016/j.atmosenv.2005.03.045>
- Emery, H. E., & Fulweiler, R. W. (2014). *Spartina alterniflora* and invasive *Phragmites australis* stands have similar greenhouse gas emissions in a New England marsh. *Aquatic Botany*, 116, 83–92. <https://doi.org/10.1016/j.aquabot.2014.01.010>
- EPA. (2021). US Environmental Protection Agency. Air quality system data mart: MassDEP Met Station in Truro (25–001–0002). https://aqs.epa.gov/aqsweb/airdata/download_files.html
- Evans, C. D., Peacock, M., Baird, A. J., Artz, R. R. E., Burden, A., Callaghan, N., Chapman, P. J., Cooper, H. M., Coyle, M., Craig, E., Cumming, A., Dixon, S., Gauci, V., Grayson, R. P., Helfter, C., Heppell, C. M., Holden, J., Jones, D. L., Kaduk, J., ... Morrison, R. (2021). Overriding water table control on managed peatland greenhouse gas emissions. *Nature*, 593, 548–552. <https://doi.org/10.1038/s41586-021-03523-1>
- Fargione, J. E., Bassett, S., Boucher, T., Bridgman, S. D., Conant, R. T., Cook-Patton, S. C., Ellis, P. W., Falcucci, A., Fourqurean, J. W., Gopalakrishna, T., Gu, H., Henderson, B., Hurteau, M. D., Kroeger, K. D., Kroeger, T., Lark, T. J., Leavitt, S. M., Lomax, G., McDonald, R. I., ... Griscom, B. W. (2018). Natural climate solutions for the United States. *Science Advances*, 4(11), 1–15. <https://doi.org/10.1126/sciadv.aat1869>
- Forbrich, I., Giblin, A. E., & Hopkinson, C. S. (2018). Constraining marsh carbon budgets using long-term C burial and contemporary atmospheric CO₂ fluxes. *Journal of Geophysical Research: Biogeosciences*, 123(3), 867–878. <https://doi.org/10.1002/2017JG004336>
- Hatala, J. A., Detto, M., & Baldocchi, D. D. (2012). Gross ecosystem photosynthesis causes a diurnal pattern in methane emission from rice. *Geophysical Research Letters*, 39(6), 1–5. <https://doi.org/10.1029/2012GL051303>
- Hazelton, E. L. G., Mozdzer, T. J., Burdick, D. M., Kettenring, K. M., & Whigham, D. F. (2014). *Phragmites australis* management in the United States: 40 years of methods and outcomes. *AoB Plants*, 6, 1–19. <https://doi.org/10.1093/aobpla/plu001>
- Herr, D., & Landis, E. (2016). *Coastal blue carbon ecosystems-opportunities for nationally defined contributions policy brief*. International Union for the Conservation of Nature and the Nature Conservancy.
- Hirota, M., Senga, Y., Seike, Y., Nohara, S., & Kunii, H. (2007). Fluxes of carbon dioxide, methane and nitrous oxide in two contrastive fringing zones of coastal lagoon, Lake Nakaumi, Japan. *Chemosphere*, 68(3), 597–603. <https://doi.org/10.1016/j.chemosphere.2007.01.002>
- Holmquist, J. R., Windham-Myers, L., Bliss, N., Crooks, S., Morris, J. T., Megonigal, J. P., Troxler, T., Weller, D., Callaway, J., Drexler, J., Ferner, M. C., Gonnea, M. E., Kroeger, K. D., Schile-Beers, L., Woo, I., Buffington, K., Breithaupt, J., Boyd, B. M., Brown, L. N., ... Woodrey, M. (2018). Accuracy and precision of tidal wetland soil carbon mapping in the conterminous United States. *Scientific Reports*, 8(May), 1–16. <https://doi.org/10.1038/s41598-018-26948-7>
- IPCC. (2014). *2013 supplement to the 2006 IPCC guidelines for National Greenhouse gas Inventories: Wetlands* (T. Hiraishi, T. Krug, K. Tanabe, N. Srivastava, J. Baasansuren, M. Fukuda, & T. G. Troxler [Eds.]). IPCC.
- IPCC. (2021). Climate change 2021: The physical science basis. In V. Masson-Delmotte, P. Zhai, A. Pirani, S. L. Connors, C. Péan, S. Berger, N. Caud, Y. Chen, L. Goldfarb, M. I. Gomis, M. Huang, K. Leitzell, E. Lonnoy, J. B. R. Matthews, T. K. Maycock, T. Waterfield, O. Yelekçi, R. Yu, & B. Zhou (Eds.), *Contribution of working group I to the sixth assessment report of the Intergovernmental Panel on Climate Change*. Cambridge University.
- Ibisch, P. L., Hoffmann, M. T., Kreft, S., Pe'er, G., Kati, V., Biber-Freudenberger, L., DellaSala, D. A., Vale, M. M., Hobson, P. R., & Selva, N. (2016). A global map of roadless areas and their conservation status. *Science*, 354(6318), 1423–1427. <https://doi.org/10.1126/science.aaf7166>
- Juszczak, R. (2013). Biases in methane chamber measurements in peatlands. *International Agrophysics*, 27(2), 159–168. <https://doi.org/10.2478/v10247-012-0081-z>
- Kim, J., Chaudhary, D. R., Lee, J., Byun, C., Ding, W., Kwon, B. O., Khim, J. S., & Kang, H. (2020). Microbial mechanism for enhanced methane emission in deep soil layer of *Phragmites*-introduced tidal marsh. *Environment International*, 134(November 2019), 105251. <https://doi.org/10.1016/j.envint.2019.105251>
- Kim, Y., Johnson, M. S., Knox, S. H., Black, T. A., Dalmagro, H. J., Kang, M., Kim, J., & Baldocchi, D. (2020). Gap-filling approaches for eddy covariance methane fluxes: A comparison of three machine learning algorithms and a traditional method with principal component analysis. *Global Change Biology*, 26(3), 1499–1518. <https://doi.org/10.1111/gcb.14845>
- Kljun, N., Calanca, P., Rotach, M. W., & Schmid, H. P. (2015). A simple two-dimensional parameterisation for flux footprint prediction (FFP). *Geoscientific Model Development*, 8(11), 3695–3713. <https://doi.org/10.5194/gmd-8-3695-2015>
- Knox, S. H., Jackson, R. B., Poulter, B., McNicol, G., Fluet-Chouinard, E., Zhang, Z., Hugelius, G., Bousquet, P., Canadell, J. G., Saunio, M., Papale, D., Chu, H., Keenan, T. F., Baldocchi, D., Torn, M. S., Mammarella, I., Trotta, C., Aurela, M., Bohrer, G., ... Zona, D. (2019). FluXNET-CH4 synthesis activity objectives, observations, and future directions. *Bulletin of the American Meteorological Society*, 100(12), 2607–2632. <https://doi.org/10.1175/BAMS-D-18-0268.1>
- Koebisch, F., Winkel, M., Liebner, S., Liu, B., Westphal, J., Schmiedinger, I., Spitz, A., Gehre, M., Jurasinski, G., Köhler, S., Unger, V., Koch, M., Sachs, T., & Böttcher, M. (2019). Sulfate deprivation triggers high methane production in a disturbed and rewetted coastal peatland. *Biogeosciences*, 16, 1937–1953. <https://doi.org/10.5194/bg-16-1937-2019>
- Krauss, K. W., Holm, G. O., Perez, B. C., McWhorter, D. E., Cormier, N., Moss, R. F., Johnson, D. J., Neubauer, S. C., & Rainey, R. C. (2016). Component greenhouse gas fluxes and radiative balance from two deltaic marshes in Louisiana: Pairing chamber techniques and eddy covariance. *Journal of Geophysical Research: Biogeosciences*, 121(6), 1503–1521. <https://doi.org/10.1002/2015JG003224>
- Kroeger, K. D., Crooks, S., Moseman-Valtierra, S., & Tang, J. (2017). Restoring tides to reduce methane emissions in impounded wetlands: A new and potent blue carbon climate change intervention. *Scientific Reports*, 7(1), 1–12. <https://doi.org/10.1038/s41598-017-12138-4>
- Lenth, R. V. (2020). Emmeans: Estimated marginal means, aka least-squares means. R package version 1.5.3. <https://cran.r-project.org/package=emmeans>
- Li, X., Bellerby, R., Craft, C., & Widney, S. E. (2018). Coastal wetland loss, consequences, and challenges for restoration. *Anthropocene Coasts*, 15, 1–15. <https://doi.org/10.1139/anc-2017-0001>
- Lu, M., Caplan, J. S., Barker, J. D., Langley, J. A., Mozdzer, T. J., Drake, B. G., & Megonigal, J. P. (2016). Allometry data and equations for coastal marsh plants. *Ecology*, 97(12), 3554. <https://doi.org/10.1002/ecy>
- Lu, W., Xiao, J., Liu, F., Zhang, Y., Liu, C., & Lin, G. (2017). Contrasting ecosystem CO₂ fluxes of inland and coastal wetlands: A meta-analysis of eddy covariance data. *Global Change Biology*, 23(3), 1180–1198. <https://doi.org/10.1111/gcb.13424>
- Luo, M., Huang, J. F., Zhu, W. F., & Tong, C. (2019). Impacts of increasing salinity and inundation on rates and pathways of organic carbon mineralization in tidal wetlands: A review. *Hydrobiologia*, 827(1), 31–49. <https://doi.org/10.1007/s10750-017-3416-8>

- Martin, R. M., & Moseman-Valtierra, S. (2015). Greenhouse gas fluxes vary between phragmites Australis and native vegetation zones in coastal wetlands along a salinity gradient. *Wetlands*, 35(6), 1021–1031. <https://doi.org/10.1007/s13157-015-0690-y>
- Mauder, M., & Foken, T. (2006). Impact of post-field data processing on eddy covariance flux estimates and energy balance closure. *Meteorologische Zeitschrift*, 15, 597–609.
- McLeod, E., Chmura, G. L., Bouillon, S., Salm, R., Björk, M., Duarte, C. M., Lovelock, C. E., Schlesinger, W. H., & Silliman, B. R. (2011). A blueprint for blue carbon: Toward an improved understanding of the role of vegetated coastal habitats in sequestering CO₂. *Frontiers in Ecology and the Environment*, 9(10), 552–560. <https://doi.org/10.1890/110004>
- Moncrieff, J. B., Massheder, J. M., de Bruin, H., Elbers, J., Friborg, T., Heusinkveld, B., Kabat, P., Scott, S., Soegaard, H., & Verhoef, A. (1997). A system to measure surface fluxes of momentum, sensible heat, water vapour and carbon dioxide. *Journal of Hydrology*, 188–189(1–4), 589–611. [https://doi.org/10.1016/S0022-1694\(96\)03194-0](https://doi.org/10.1016/S0022-1694(96)03194-0)
- Moseman-Valtierra, S., Abdul-Aziz, O. I., Tang, J., Ishtiaq, K. S., Morkeski, K., Mora, J., Quinn, R. K., Martin, R. M., Egan, K., Brannon, E. Q., Carey, J., & Kroeger, K. D. (2016). Carbon dioxide fluxes reflect plant zonation and belowground biomass in a coastal marsh. *Ecosphere*, 7(11), e01560. <https://doi.org/10.1002/ecs2.1560>
- Mozdzer, T. J., & Megonigal, J. P. (2013). Increased methane emissions by an introduced Phragmites australis lineage under global change. *Wetlands*, 33(4), 609–615. <https://doi.org/10.1007/s13157-013-0417-x>
- National Academies of Science, Engineering, and Medicine (NASEM). (2019). *Negative emissions technologies and reliable sequestration: A research agenda*. National Academies Press. <https://doi.org/10.17226/25259>
- Needleman, B. A., Emmer, I. M., Emmett-Mattox, S., Crooks, S., Megonigal, J. P., Myers, D., Oreska, M. P. J., & McGlathery, K. (2018). The science and policy of the verified carbon standard methodology for tidal wetland and seagrass restoration. *Estuaries and Coasts*, 41(8), 2159–2171. <https://doi.org/10.1007/s12237-018-0429-0>
- Neubauer, S. C., & Megonigal, J. P. (2015). Moving beyond global warming potentials to quantify the climatic role of ecosystems. *Ecosystems*, 18(6), 1000–1013. <https://doi.org/10.1007/s10021-015-9879-4>
- O'Keefe Suttles, J. A., Eagle, M., Mann, A., Spivak, A. C., Sanks, K., Roberts, D., & Kroeger, K. D. (2021). *Collection, analysis, and age-dating of sediment cores from natural and restored salt marshes on Cape Cod, Massachusetts, 2015–16: U.S. Geological Survey data release*. <https://doi.org/10.5066/P9R154DY>
- O'Keefe Suttles, J. A., Eagle, M., Mann, A., Wang, F., Tang, J., Roberts, D., Sanks, K., Smith, T. P., & Kroeger, K. D. (2021). *Collection, analysis, and age-dating of sediment cores from Herring River wetlands and other nearby wetlands in Wellfleet, Massachusetts, 2015–17: U.S. Geological Survey data release*. <https://doi.org/10.5066/P95RXPHB>
- O'Keefe Suttles, J.A., M. Eagle, Martin, R.M., Moseman-Valtierra, S., & Kroeger, K. D. (2022). *Static chamber gas fluxes and carbon and nitrogen isotope content of age-dated sediment cores from a Phragmites wetland in Sage Lot Pond, Massachusetts, 2013–2015: U.S. Geological Survey data release*. <https://doi.org/10.5066/P9JM751N>
- O'Keefe Suttles, J.A., M.J. Eagle, R. Sanders-DeMott, S.K. Nick, T.W. Brooks, A.G. Mann, and K.D. Kroeger. (2022) *Continuous Water Level, Salinity, and Temperature Data from Monitoring Wells in Wetlands on the South Shore of Cape Cod, Massachusetts, 2020: U.S. Geological Survey data release*. <https://doi.org/10.5066/P9T1KOTW>
- O'Keefe Suttles, J. A., Gonneea, M. E., Brosnahan, S. M., Mann, A. G., Brooks, T. W., Kroeger, K. D., Medeiros, K., Smith, T. P., Wang, F., & Tang, J. (2020). Continuous monitoring data from Herring River wetlands. In *Cape Cod, Massachusetts, 2015 to 2020*. <https://doi.org/10.5066/P9R45RTR>
- Papale, D., Reichstein, M., Aubinet, M., Canfora, E., Bernhofer, C., Kutsch, W., Longdoz, B., Rambal, S., Valentini, R., Vesala, T., & Yakir, D. (2006). Towards a standardized processing of net ecosystem exchange measured with eddy covariance technique: Algorithms and uncertainty estimation. *Biogeosciences*, 3(4), 571–583. <https://doi.org/10.5194/bg-3-571-2006>
- Poffenbarger, H. J., Needelman, B. A., & Megonigal, J. P. (2011). Salinity influence on methane emissions from tidal marshes. *Wetlands*, 31(5), 831–842. <https://doi.org/10.1007/s13157-011-0197-0>
- Portnoy, J. W. (1999). Salt marsh diking and restoration: Biogeochemical implications of altered wetland hydrology. *Environmental Management*, 24(1), 111–120. <https://doi.org/10.1007/s002679900219>
- R Core Team. (2022). *R: A language and environment for statistical computing*. R Foundation for Statistical Computing. <http://www.r-project.org/>
- Reichstein, M., Falge, E., Baldocchi, D., Papale, D., Aubinet, M., Berbigier, P., Bernhofer, C., Buchmann, N., Gilmanov, T., Granier, A., Grünwald, T., Havránková, K., Ilvesniemi, H., Janous, D., Knohl, A., Laurila, T., Lohila, A., Loustau, D., Matteucci, G., ... Valentini, R. (2005). On the separation of net ecosystem exchange into assimilation and ecosystem respiration: Review and improved algorithm. *Global Change Biology*, 11(9), 1424–1439. <https://doi.org/10.1111/j.1365-2486.2005.001002.x>
- Roman, C. T., Niering, W. A., & Warren, R. S. (1984). Salt marsh vegetation change in response to tidal restriction. *Environmental Management*, 8(2), 141–149. <https://doi.org/10.1007/BF01866935>
- Rosentreter, J. A., Al-Haj, A. N., Fulweiler, R. W., & Williamson, P. (2021). Methane and nitrous oxide emissions complicate coastal blue carbon assessments. *Global Biogeochemical Cycles*, 35, 1–8. <https://doi.org/10.1029/2020gb006858>
- Sanders-DeMott, R., Eagle, M. J., Kroeger, K. D., Wang, F., Brooks, T. W., O'Keefe Suttles, J. A., Nick, S. K., Mann, A. G., & Tang, J. (2022). Carbon dioxide and methane fluxes with supporting environmental data from coastal wetlands across Cape Cod, Massachusetts. U.S. Geological Survey data release, <https://doi.org/10.5066/P9RRL3T0>
- Schäfer, K. V. R., Duman, T., Tomasicchio, K., Tripathee, R., & Sturtevant, C. (2019). Carbon dioxide fluxes of temperate urban wetlands with different restoration history. *Agricultural and Forest Meteorology*, 275(2018), 223–232. <https://doi.org/10.1016/j.agrfor.2019.05.026>
- Schenck, F. R., Hanley, T. C., Beighley, R. E., & Hughes, A. R. (2018). Phenotypic variation among invasive Phragmites australis populations does not influence salinity tolerance. *Estuaries and Coasts*, 41(3), 896–907. <https://doi.org/10.1007/s12237-017-0318-y>
- Shannon, J. (2018). *ecoFlux: Functions for ecological flux studies including sap flux and soil/stem C efflux (0.3.1)*. <https://rdr.io/github/jpsahanno/ecoFlux/>
- United Nations/Framework Convention on Climate Change. (2015). *Adoption of the Paris Agreement, 21st Conference of the Parties*. United Nations U.N. Doc. FCCC/CP/2015/L.9/Rev/1.
- United States Drought Monitor (USDM). (2021). *United States Drought Monitor*. National Drought Mitigation Center (NDMC), the U.S. Department of Agriculture (USDA) and the National Oceanic and Atmospheric Administration (NOAA). <https://droughtmonitor.unl.edu/DmData/TimeSeries.a>
- van den Berg, M., Ingwersen, J., Lamers, M., & Streck, T. (2016). The role of phragmites in the CH₄ and CO₂ fluxes in a minerotrophic peatland in Southwest Germany. *Biogeosciences*, 13(21), 6107–6119. <https://doi.org/10.5194/bg-13-6107-2016>
- van den Berg, M., van den Elzen, E., Ingwersen, J., Kosten, S., Lamers, L. P. M., & Streck, T. (2020). Contribution of plant-induced pressurized flow to CH₄ emission from a phragmites fen. *Scientific Reports*, 10(1), 12304. <https://doi.org/10.1038/s41598-020-69034-7>

- Van Der Nat, F. J., & Middelburg, J. J. (1998). Effects of two common macrophytes on methane dynamics in freshwater sediments. *Biogeochemistry*, 43(1), 79–104. <https://doi.org/10.1023/A:1006076527187>
- Van der Nat, F. J., & Middelburg, J. J. (2000). Methane emission from tidal freshwater marshes. *Biogeochemistry*, 49(2), 103–121. <https://doi.org/10.1023/A:1006333225100>
- Van Der Nat, F. J., Middelburg, J. J., Van Meteren, D., & Wielemakers, A. (1998). Diel methane emission patterns from *Scirpus lacustris* and *Phragmites australis*. Annette Wielemakers published by: Springer stable. *Biogeochemistry*, 41(1), 1–22. <https://www.jstor.org/stable/1469306>
- Van Dijk, A. I. J. M., & Dolman, A. J. (2004). Estimates of CO₂ uptake and release among European forests based on eddy covariance data. *Global Change Biology*, 10(9), 1445–1459. <https://doi.org/10.1111/j.1365-2486.2004.00831.x>
- Vasquez, E. A., Glenn, E. P., Guntenspergen, G. R., Brown, J. J., & Nelson, S. G. (2006). Salt tolerance and osmotic adjustment of *Spartina alterniflora* (Poaceae) and the invasive M haplotype of *Phragmites australis* (Poaceae) along a salinity gradient. *American Journal of Botany*, 93(12), 1784–1790. <https://doi.org/10.3732/ajb.93.12.1784>
- Vázquez-Lule, A., & Vargas, R. (2021). Biophysical drivers of net ecosystem and methane exchange across phenological phases in a tidal salt marsh. *Agricultural and Forest Meteorology*, 300(June 2020), 108309. <https://doi.org/10.1016/j.agrformet.2020.108309>
- Vickers, D., & Mahrt, L. (1997). Quality control and flux sampling problems for tower and aircraft data. *Journal of Atmospheric and Oceanic Technology*, 14(3), 512–526. [https://doi.org/10.1175/1520-0426\(1997\)014<0512:QCAFSP>2.0.CO;2](https://doi.org/10.1175/1520-0426(1997)014<0512:QCAFSP>2.0.CO;2)
- Villa, J. A., Ju, Y., Stephen, T., Rey-Sanchez, C., Wrighton, K. C., & Bohrer, G. (2020). Plant-mediated methane transport in emergent and floating-leaved species of a temperate freshwater mineral-soil wetland. *Limnology and Oceanography*, 65(7), 1635–1650. <https://doi.org/10.1002/lno.11467>
- Wang, C., Tong, C., Chambers, L. G., & Liu, X. (2017). Identifying the salinity thresholds that impact greenhouse gas production in subtropical tidal freshwater marsh soils. *Wetlands*, 37(3), 559–571. <https://doi.org/10.1007/s13157-017-0890-8>
- Wang, Z. A., Kroeger, K. D., Ganju, N. K., Gonneea, M. E., & Chu, S. N. (2016). Intertidal salt marshes as an important source of inorganic carbon to the coastal ocean. *Limnology and Oceanography*, 61(5), 1916–1931. <https://doi.org/10.1002/lno.10347>
- Webb, E. K., Pearman, G. I., & Leuning, R. (1980). Correction of flux measurements for density effects due to heat and water vapour transfer. *Quarterly Journal of the Royal Meteorological Society*, 106(447), 85–100. <https://doi.org/10.1002/qj.49710644707>
- Weston, N. B., Dixon, R. E., & Joye, S. B. (2006). Ramifications of increased salinity in tidal freshwater sediments: Geochemistry and microbial pathways of organic matter mineralization. *Journal of Geophysical Research*, 111(G1), G01009. <https://doi.org/10.1029/2005JG000071>
- Weston, N. B., Neubauer, S. C., Velinsky, D. J., & Vile, M. A. (2014). Net ecosystem carbon exchange and the greenhouse gas balance of tidal marshes along an estuarine salinity gradient. *Biogeochemistry*, 120(1–3), 163–189. <https://doi.org/10.1007/s10533-014-9989-7>
- Wickham, H. (2016). *ggplot2: Elegant graphics for data analysis* (p. ISBN 978-3-319-24277-4). Springer-Verlag New York. <https://ggplot2.tidyverse.org>
- Wickham, H., François, R., Henry, L., & Müller, K. (2020). Dplyr: A grammar of data manipulation. R package version 1.0.2. <https://cran.r-project.org/package=dplyr>
- Wilczak, J. M., Oncley, S. P., & Stage, S. A. (2001). Sonic anemometer tilt correction algorithms. *Boundary-Layer Meteorology*, 99, 127–150.
- Windham, L. (2001). Comparison of biomass production and decomposition between *Phragmites australis* (common reed) and *Spartina patens* (salt hay grass) in brackish tidal marshes of New Jersey, USA. *Wetlands*, 21(2), 179–188. [https://doi.org/10.1672/0277-5212\(2001\)021\[0179:COBPAD\]2.0.CO;2](https://doi.org/10.1672/0277-5212(2001)021[0179:COBPAD]2.0.CO;2)
- Windham-Myers, L., Cai, W.-J., Alin, S., Andersson, A., Crosswell, J., Dunton, K. H., Hernandez-Ayon, J. M., Herrmann, M., Hinson, A. L., Hopkinson, C. S., Howard, J., Hu, X., Knox, S. H., Kroeger, K., Lagomasino, D., Megonigal, P., Najjar, R. G., Paulsen, M.-L., Peteet, D., ... Watson, E. B. (2018). Chapter 15: Tidal wetlands and estuaries. In N. Cavallaro, G. Shrestha, R. Birdsey, M. A. Mayes, R. G. Najjar, S. C. Reed, P. Romero-Lankao, & Z. Zhu (Eds.), *Second state of the carbon cycle report (SOCCR2): A sustained assessment report* (pp. 596–648). U.S. Global Change Research Program. <https://doi.org/10.7930/SOCCR2.2018.Ch15>
- Wutzler, T., Lucas-Moffat, A., Migliavacca, M., Knauer, J., Sickel, K., Šigut, L., Menzer, O., & Reichstein, M. (2018). *Basic and extensible post-processing of eddy covariance flux data with REddyProc* (pp. 1–39). Biogeosciences Discussions. <https://doi.org/10.5194/bg-2018-56>

SUPPORTING INFORMATION

Additional supporting information may be found in the online version of the article at the publisher's website.

How to cite this article: Sanders-DeMott, R., Eagle, M. J., Kroeger, K. D., Wang, F., Brooks, T. W., O'Keefe Suttles, J. A., Nick, S. K., Mann, A. G., & Tang, J. (2022). Impoundment increases methane emissions in *Phragmites*-invaded coastal wetlands. *Global Change Biology*, 28, 4539–4557. <https://doi.org/10.1111/gcb.16217>